# Adhesion strength of titanium particles to alumina substrates: a combined cold spray and LIPIT study

Imbriglio, S. I.; Hassani-Gangaraj, M.; Veysset, D.; Aghasibeig, M.; Gauvin, R.; Nelson, K. A.; Schuh, C. A.; Chromik, R. R.



**Publisher's version / Version de l'éditeur:**
https://doi.org/10.1016/j.surfcoat.2019.01.071
*Surface & Coatings Technology, 361, pp. 403-412, 2019-01-23*

Elsevier Editorial System(tm) for Surface and Coatings Technology
Manuscript Draft

Manuscript Number: SURFCOAT-D-18-03059R2

Title: Adhesion strength of titanium particles to alumina substrates: A combined cold spray and LIPIT study

Article Type: Full Length Article

Keywords: cold spray; impact; metal/ceramic interface; adhesion strength; substrate morphology; impact velocity

Corresponding Author: Professor Richard R Chromik, Ph.D.

Corresponding Author's Institution: McGill University

First Author: Sara I Imbriglio

Order of Authors: Sara I Imbriglio; Mostafa Hassani-Gangaraj; David Veysset; Maniya Aghasibeig; Raynald Gauvin; Keith A Nelson; Christopher A Schuh; Richard R Chromik, Ph.D.

Abstract: The cold spray process and laser-induced projectile impact test (LIPIT) are used to deposit Ti powder particles on sintered polycrystalline Al2O3. Whereas LIPIT allows real-time observations of single particle impact and measurement of particle impact velocity, cold spray rapidly and simultaneously deposits particles with a wide range of deposition velocities and sizes. By use of these two techniques, the effect of particle velocity and substrate morphology on adhesion strength of single splats is investigated. The critical velocity for deposition is identified to be approximately 580 m/s for the Ti/Al2O3 system when using LIPIT and particles of 10 µm. Above the critical velocity, flattening ratio (FR) is also evaluated and observed to be linearly dependent on the particle impact velocity. Splat adhesion testing is performed on LIPIT-deposited as well as on cold spray-deposited powder particles to measure adhesion strength. This analysis shows that adhesion strength is highly affected by local substrate surface morphology, where particles bond more weakly to relatively smooth portions of the substrate. Therefore, mechanical bonding plays a significant role in adhesion. Also, adhesion strength decreases with an increase in FR and therefore velocity. This decrease can be associated with fracture of the ceramic substrate and rebound forces.

*Highlights (for review)

**Highlights:**

- Ti splats are deposited on sintered polycrystalline $Al_2O_3$ by cold spray and LIPIT.
- LIPIT revealed that Ti splats begin to bond to $Al_2O_3$ at approximately 580 m/s.
- Flattening ratio can be used to estimate an effective velocity for single splats.
- Adhesion strength is inversely proportional to flattening ratio for cold spray splats.
- Areas on the substrate with smaller $Al_2O_3$ grains lead to higher adhesion strength.

# Adhesion strength of titanium particles to alumina substrates: A combined cold spray and LIPIT study

**S. Imbriglio[a], M. Hassani-Gangaraj[b], D. Veysset[c], M. Aghasibeig[d] R. Gauvin[a], K. A. Nelson[e], C. A. Schuh[b], R. R. Chromik[a,*]**

[a] Department of Mining and Materials Engineering, McGill University, 3610 University Street, Montreal, QC H3A 0C5, Canada

[b] Department of Materials Science and Engineering, Massachusetts Institute of Technology, 77 Massachusetts Ave, Cambridge, MA 02139, USA

[c] Institute for Soldier Nanotechnologies, Massachusetts Institute of Technology, 77 Massachusetts Ave, Cambridge, MA 02139, USA

[d] National Research Council Canada, Boucherville, QC, J4B 6Y4, Canada

[e] Department of Chemistry, Massachusetts Institute of Technology, 77 Massachusetts Ave, Cambridge, MA 02139, USA

* Corresponding author. Telephone: +1(514) 398-5686; Fax: +1 (514) 398-4492

Email address: richard.chromik@mcgill.ca

Declarations of interest: none

**Abstract**

The cold spray process and laser-induced projectile impact test (LIPIT) are used to deposit Ti powder particles on sintered polycrystalline $Al_2O_3$.  Whereas LIPIT allows real-time observations of single particle impact and measurement of particle impact velocity, cold spray rapidly and simultaneously deposits particles with a wide range of deposition velocities and sizes. By use of these two techniques, the effect of particle velocity and substrate morphology on adhesion strength of single splats is investigated. The critical velocity for deposition is identified to be approximately 580 m/s for the $Ti/Al_2O_3$ system when using LIPIT and particles of 10 µm. Above the critical velocity, flattening ratio (FR) is also evaluated and observed to be linearly dependent on the particle impact velocity. Splat adhesion testing is performed on LIPIT-deposited as well as on cold spray-deposited powder particles to measure adhesion strength. This analysis shows that adhesion strength is highly affected by local substrate surface morphology, where particles bond more weakly to relatively smooth portions of the substrate.  Therefore, mechanical bonding plays a significant role in adhesion. Also, adhesion strength decreases with an increase in FR and therefore velocity. This decrease can be associated with fracture of the ceramic substrate and rebound forces.

**Keywords** cold spray; impact; metal/ceramic interface; adhesion strength; substrate morphology; impact velocity

## 1. Introduction

Cold spray coatings are formed by high-velocity impact of solid powder particles on a substrate. Metal/metal interfaces between particles or the particles and substrate have the strongest bonding when jetting occurs; jetting leads to metallurgical bonding by creating clean metallic surfaces and/or removing the native oxide layer [1-5]. Besides metallurgical bonding, mechanical bonding can also lead to particle deposition [2, 4, 6]. For jetting to occur, particles must travel above a critical velocity, which is the minimum particle impact velocity leading to adhesion. This velocity has been estimated for many material systems [7, 8] and it has been recently directly measured through real time observations [9]. For identical metallic counterparts, critical velocity has been reported to be influenced by melting temperature, mechanical strength, density and powder size [1, 8, 10]. When bonding dissimilar metallic materials, deposition is highly influenced by differences in hardness and density [11, 12].

While metal/metal interfaces created by cold spray are well understood, the necessary conditions for bonding of cold sprayed metal powder particles on ceramic substrates remain unclear [11]. Use of cold spray for metal matrix composite (MMC) coatings with ceramic reinforcement [13] and metal coatings on ceramic substrates [14-22] creates a need to characterize bonding mechanisms and deposition conditions for metal/ceramic systems, especially since no consensus has been established regarding the bonding mechanism in cold sprayed metal/ceramic interfaces. For cold sprayed MMCs, mechanical bonding by deformation of the metal around rigid ceramic particles is a proposed bonding mechanism, which depends on the shape and roughness of the ceramic phase [23]. In the deposition of metal coatings on ceramic substrates, mechanical interlocking has been shown to contribute to bonding when a rough substrate is used in an Al/$Al_2O_3$ interface [14, 24]. Yet, metal particles have also been successfully deposited on smooth ceramic substrates where mechanical bonding is not possible [15, 17, 19, 22, 25, 26]. Therefore, chemical bonding may also occur in metal/ceramic interfaces created by cold spray. The chemical interaction between atoms at the interface is attributed to amorphisation of the metal and atomic intermixing resulting in a heteoepitaxial relationship [14, 15, 20, 22, 24]. To achieve adhesion, the key parameters identified are the impact velocity as well as the difference in hardness and mechanical properties of the metal and ceramic [24]. Due to a poor understanding of the above mentioned key parameters in forming a chemical or mechanical bond, deposition conditions to achieve adhesion in metal/ceramic interfaces have yet to be identified.

Critical velocity is typically investigated experimentally by two techniques. For example, the deposition efficiency of a full coating under different spray conditions can be compared. Alternatively, single particle impacts can be characterized for specified spray conditions to determine whether particles bonded or rebounded using a wipe test [27]. In neither case is critical velocity directly measured, but rather is back-calculated as a function of process parameters that lead to a certain level of deposition efficiency. In cold spray, particle velocity is varied by either increasing initial gas pressure or gas pre-heat temperature. An increase in gas pre-heat temperature results in an increase in thermal softening of the powder prior to impact [11]. Critical velocity also tends to decrease with an increase in gas pre-heat temperature [28, 29]. In addition, the velocity of the powder in the center of the jet is higher than the velocity near the edges [30, 31]. To avoid these issues in identifying an approximate critical velocity, a laser-induced projectile impact test (LIPIT) is used in this work.

LIPIT is an *in situ* technique used to identify the impact velocity of single particles [9, 32-35]. This technique uses a high-frame-rate camera to image the trajectory of a single particle that has been accelerated from a platform with a laser pulse [9, 36]. From the images, particle velocity is calculated and the adhesion or rebound of a single micron-sized particle is observed [9, 36, 37]. While particle in-flight velocity can be measured using commercially available systems in cold spray, these are not designed to measure impact velocity leading to adhesion. In what follows, LIPIT is used to deposit Ti powder particles onto sintered high purity polycrystalline $Al_2O_3$ substrates to isolate the effect of impact velocity from other influencing factors in this metal/ceramic interface. Ti/$Al_2O_3$ interfaces have been selected as a model metal/ceramic system due to their promising results in previous literature [17, 38]. The critical velocity for deposition of Ti onto the surface of $Al_2O_3$ is approximated, and by studying the morphology of bonded particles, the effect of velocity on flattening ratio (FR) is identified. Also, the effect of surface morphology on adhesion strength, at similar particle velocities, is investigated where adhesion strength was measured by splat adhesion testing [39]. However, since selective deposition of many particles at certain velocities on certain substrate morphologies is tedious by LIPIT, it is difficult to identify a general trend between adhesion strength and velocity. For this, cold sprayed particles are used to study many particles deposited simultaneously.

## 2. Research Methodology

In LIPIT, micron-sized, commercially pure, spherical Ti powder particles (Gr 1, AP&C, Quebec, Canada) are accelerated from a launch pad composed of a 210 μm thick glass substrate sputter-coated with 60 nm of gold, then coated with an elastomeric polyurea coating about 30 μm thick [9]. Details regarding the LIPIT system [9] and additional characterization of the Ti powder particles [38] have been presented elsewhere. The Ti powder, suspended in ethanol, is spread over the surface of the polymeric coating and is allowed to dry. The laser pulse (Nd:YAG laser pulse of 10 ns and 532 nm wavelength) causes ablation of the gold film and expansion of the polymer. In consequence, rapid acceleration of the Ti powder particle towards the $Al_2O_3$

substrate (AD-995, CoorsTek, Arkansas, USA) is achieved. Depending on the laser pulse energy, Ti powder particles can be accelerated to velocities between 350 and 995 m/s. A 16-frame high speed camera (SIMX 16, Specialised Imaging) is used to capture the particle/substrate impact. Velocities are measured by comparing the distance travelled from one frame to the other knowing the interframe time [35].

Powder particles with an average diameter of 10±1 μm are selected and launched. To select powder of a specific size, a secondary CCD camera is used. These powder particles are launched at $Al_2O_3$ target substrates cut from large sintered blocks using a diamond blade on a precision cutter to dimensions of approximately 2-3 x 12.5 x 10 $mm^3$. It is ensured that the edge of 2-3 mm, on which the metallic powder is to be deposited, is not exposed to the blade, and the as-received sintered substrate surface morphology is maintained. The sintered blocks are fabricated with a wide range of particle sizes. This causes local variations in the surface morphology of the substrates. There are granular portions of the substrate with a series of fine peaks and valleys due to small sintered grains and portions that are comparatively smooth and flat with larger grains. In [38], the local heterogeneity of this as-received $Al_2O_3$ substrate was further characterized and associated to a reduced peak height ($R_{pk}$) roughness value of 0.78 ± 0.38 μm. Surface features are observable in SEM images as shown in Fig. 1.

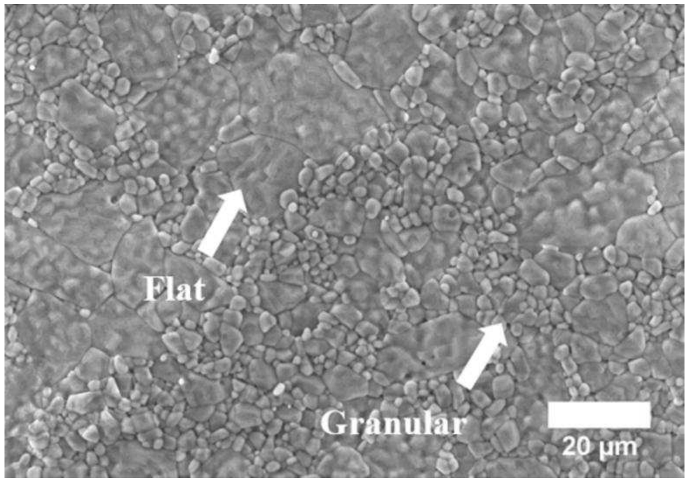


**Fig. 1.** Surface morphology of the $Al_2O_3$ substrate. Portions of the substrate include large grains which make the substrate flatter than areas that include several small grains. Areas with small grains are identified as granular while areas with large grains are identified as flat.

The same as-received Ti powder (with the full particle size distribution) is used for deposition of single particles by cold spray (PCS-800, Plasma Giken, Saitama, Japan) onto the bulk $Al_2O_3$ substrates. The cold spray gun is mounted on a robotic arm that scans the surface of the substrate during the spray at a traverse speed of 1 m/s. The standoff distance is 30 mm. The maximum initial gas pressure and gas pre-heat temperature for this cold spray system are 4.9 MPa and 800°C. For simplicity, throughout the article, gas pre-heat temperature and initial gas pressure are referred to as gas temperature and gas pressure. To reach a wide range of velocities by cold spray, two cold spray nozzle configurations are used. The "long nozzle" (PG PNFC-012-30, Plasma Giken, Saitama, Japan)'s geometry renders higher gas velocities and therefore higher powder velocities than the "standard nozzle" (PG PNFC2-010-30S, Plasma Giken, Saitama, Japan) for identical spray conditions (i.e. gas temperature and pressure).

Using the standard nozzle, the initial gas pressure is maintained at 4.0 MPa with a gas pre-heat temperature of either 400, 600 or 800°C. An increase in gas temperature is known to cause an increase in velocity [40, 41]. The long nozzle configuration is used to investigate the effect of gas temperature on FR and adhesion strength as well as to deposit particles at very high velocities using the highest gas pressure and temperature for this spray system. Using the long nozzle, the maximum gas pressure of 4.9 MPa is maintained for gas temperatures of 450 and 800°C. For each spray conditions, inflight particle velocity measurements at the standoff distance are taken using a time of flight particle diagnosis system (Coldspraymeter, Tecnar Automation, Canada). While this velocity measurement represents the in-flight velocity of the particles, it might not reflect the particle impact velocity due to the bow shock effect, which is the high-pressure region formed near the substrate. The gas pressure and temperature of 4.9 MPa and 450°C using the long nozzle give an average velocity of 695 ± 136 m/s which is effectively identical to the average velocity achieved with the standard nozzle configuration using a gas pressure of 4.0 MPa and gas temperature of 800°C measured at 692 ± 133 m/s. The long nozzle deposition condition of 4.9 MPa and 450°C is specifically selected to deposit the Ti powder particles at the lowest possible temperature while maintaining an impact velocity comparable to that achieved using the standard nozzle with a gas pressure and temperature of 4.0 MPa and 800°C. Increasing the gas pressure is necessary to ensure that the lowest temperature is used. These conditions are used to understand the effect of temperature on measurements of adhesion strength and flattening ratio.

To better understand the role of temperature in the cold spray system, a numerical model was used. Particle temperature ($T_p$) at the exit of the nozzle is estimated by eq. 1 [42] where the differential equation is solved by the Euler method along the length of the nozzle. In the model, the particle specific heat ($c_p$) , density ($\rho_p$) and particle diameter ($D_p$) are 472 J/(kg K), 4540 kg/m$^3$ and 29 μm respectively [42].

$$\frac{dT_p}{dt} = \left(T_g - T_p\right)\frac{6h}{c_p \rho_p D_p}\,, \tag{1}$$

In eq. 1, 'h' is the heat transfer coefficient which can be calculated by a semi-empirical Ranz-Marshall equation which is dependent on Reynolds number and Prandtl's number [42]. The Reynolds number and the Prandtl number are calculated using specific heat, viscosity and thermal conductivity of the gas. These gas properties are found in [43, 44] and are taken at a temperature equivalent to the average temperature of the gas and powder along the nozzle [42]. The gas flow velocity ($U_g$), pressure ($P_g$) and temperature ($T_g$) through the nozzle is obtained numerically by assuming a two dimensional flow with a gas in a quasi-one-dimensional isentropic semi-perfect state [42]. Additional details regarding the numerical simulation and assumptions made are available in [42]. For the Reynolds number, the particle velocity ($U_p$), at the exit of the nozzle, is also required and can be solved numerically by eq. 2 [42] where '$\rho_g$' is the gas density and '$C_d$' is the drag coefficient.

$$\frac{dU_p}{dt} = \frac{3}{4}\frac{C_d \rho_g}{D_p \rho_g}\left(U_g - U_p\right)\left|U_g - U_p\right|, \tag{2}$$

Following deposition, the adhesion strength is measured for all particles deposited by LIPIT and ten or more particles for each cold spray condition. The powder particles deposited by cold spray have a wide range of diameters, but the tests were performed on the particles with approximately an average initial diameter of 29 μm. The initial diameter (D), prior to deposition, can be approximated by eq. 3 [30, 45, 46].

$$D = \sqrt[3]{\frac{d^3}{FR}}\,, \qquad (3)$$

Where d is the splat diameter and FR is calculated by eq. 4 [30, 39]. The height of the splat (h) is measured by recording the height of the microscope when focusing on the top of the splat and subtracting its height when focusing on the substrate. This method is a non-destructive way to measure FR of each splat tested, and in previous work was found to correlate well with measurements from splat cross-sections [30, 39].

$$FR = \frac{d}{h} \qquad (4)$$

The particles studied by cold spray are larger than those deposited by LIPIT but are more representative of the powder size typically used in cold spray, which is also the average size of the powder used in this study. Larger particles could not be deposited by LIPIT to achieve high velocities resulting in adhesion due to limitations in the laser power. A Micro-Combi Scratch Tester (CSM Instruments, Inc, Massachusetts, USA) is used to perform splat adhesion tests [39] on the Ti splats deposited on $Al_2O_3$. Splats are scratched off the substrate by the flat face of a semi-circular specialized tip of 100 µm in diameter. A scratch length of 100 µm and speed of 150 µm/min are used for testing. To ensure that contact is maintained between the tip and the substrate, a normal force of 70 - 100 mN is used. Throughout the scratch length, the tangential force on the stylus is measured. Results typically show a baseline ($F_{T\ Baseline}$) and peak ($F_{T\ Peak}$) tangential force. The peak force corrected by subtracting the baseline is interpreted as the force required to remove the splat from the substrate. Adhesion strength, calculated by eq. 5, represents the force required to remove the splat from the substrate over the projected splat area [30, 39].

$$Adhesion\ Strength\ [MPa] = \frac{F_{T\ Peak}\ [mN] - F_{T\ Baseline}[mN]}{\pi\left(\frac{d\ [\mu m]}{2}\right)^2} * 1000 \quad (5)$$

In splat adhesion testing, the material fails at its weakest point. Therefore, failure may occur through the metal, at the interface or through the ceramic substrate. Failure through the metal is associated with a well adhering interface. Failure at the interface is typically associated with a weak bond strength. Significant failure in the ceramic typically only occurs in the presence of a pre-existing crack in the ceramic. To properly explain and characterize trends observed for different spray conditions and velocities, extensive post-test characterization is conducted. All failed interfaces are observed by light optical microscopy (LOM) following splat adhesion testing. Some splats are imaged by variable-pressure scanning electron microscopy (SEM, SU-3500, Hitachi, Tokyo, Japan) before and after splat adhesion testing. The pressure within the SEM is set to 40 Pa and the accelerating voltage to 5 kV. The low vacuum condition is used to reduced charging within the SEM caused by the non-conductive ceramic substrate [47]. Splat morphologies are compared to better understand the effect of particle impact velocity on deposition. Following splat adhesion testing, the amount of Ti remaining on the substrate and the substrate surface morphology in the failed interface are characterized to understand adhesion strength results.

## 3. Results

### 3.1. Critical velocity

With LIPIT, impact velocities resulting in bonding and rebounding can be distinguished. Fig. 2 (a) shows a typical particle impact that resulted in rebounding of the Ti splat from the $Al_2O_3$ substrate. The particle impacts the substrate with a velocity of 455 m/s between the fifth and sixth frame. Through the sixth to twelfth frame, the particle rebounds at a significantly lower velocity of 37 m/s due to its loss of kinetic energy through deformation. Fig. 2 (b) shows an impact resulting in adhesion. The particle impacts the substrate at a velocity of 631 m/s. In the fourth frame, the particle has impacted the substrate and is found to remain bonded in subsequent frames.

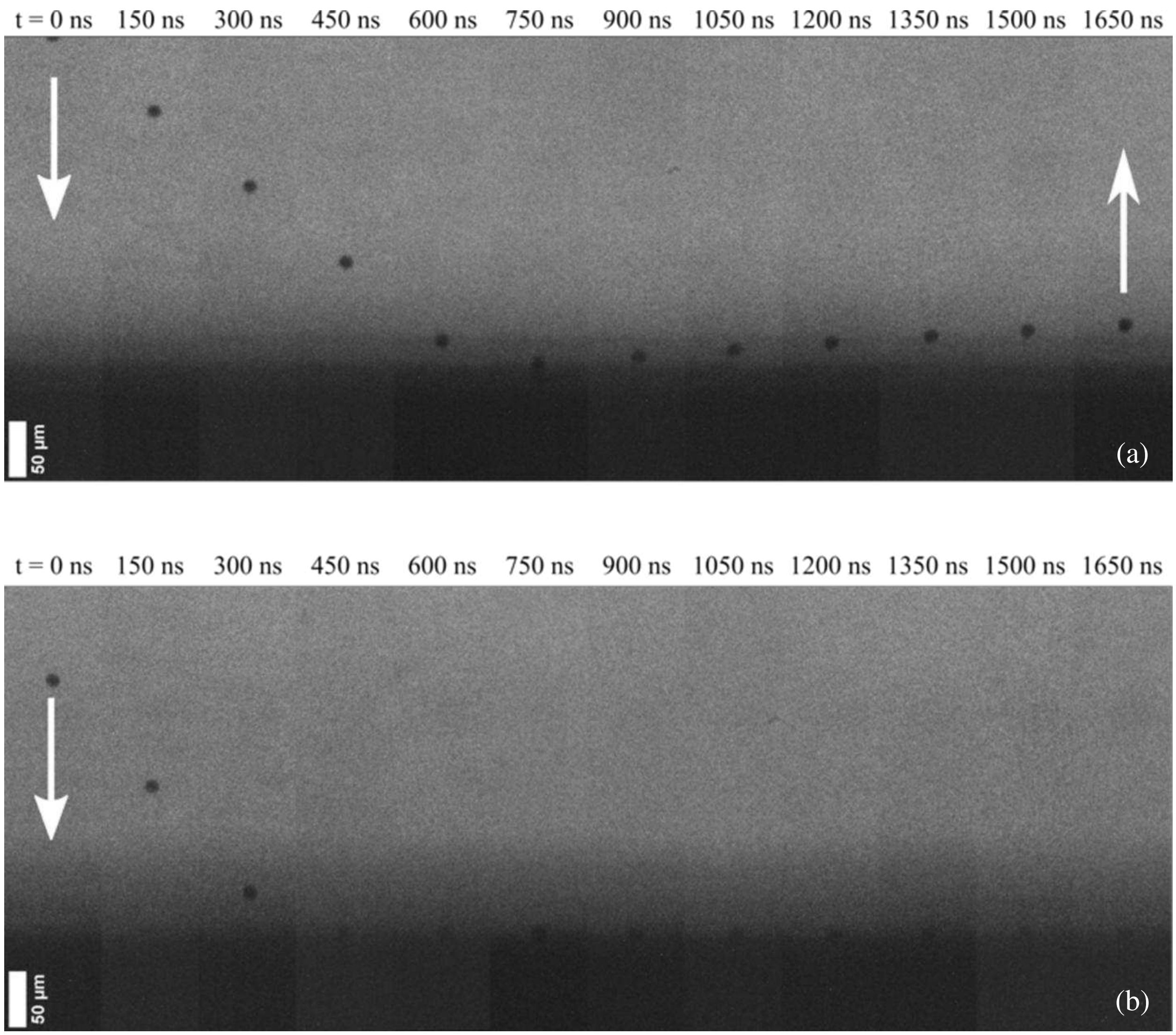


**Fig. 2.** 12 snapshots captured by the high-frame-rate camera during LIPIT (cropped to emphasize regions of interest) with a 5-ns exposure time depicting the impact of a single micron-sized Ti particle impacting the $Al_2O_3$ substrate. (a) The powder particle impacts the substrate at a

velocity of 455 m/s. Following impact, rebound occurs at 37 m/s. (b) The powder particle impacts the substrate at a velocity of 631 m/s and remains bonded to the substrate.

The coefficient of restitution (COR), which is the rebound velocity divided by the impact velocity, is plotted with respect to impact velocity to identify the critical velocity for deposition of Ti powder on $Al_2O_3$ (Fig. 3). COR decreases with increasing impact velocity until adhesion occurs, similar to experiments on matched metallic counterparts by Hassani-Gangaraj et al. [9]. For the Ti/$Al_2O_3$ interface, the lowest velocity resulting in adhesion is 580 m/s. The majority of splats impacting above this velocity adhere to the substrate. The highest velocity at which a particle rebounds is 750 m/s.

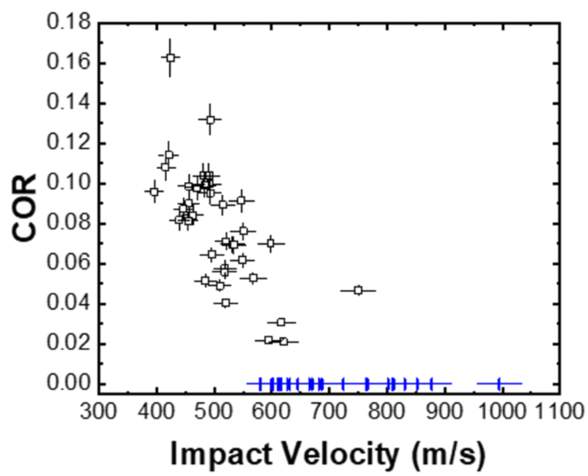


**Fig. 3.** Variation of COR with respect to impact velocity for Ti powder particles accelerated towards the $Al_2O_3$ substrate by LIPIT. Particles begin to bond to the substrate at 580 m/s. Bonded particles are depicted by blue markers on the null COR axis.

### 3.2. Characterization of bonded particles

To determine optimal deposition conditions, understanding the effect of an increase in velocity beyond the critical velocity is also necessary. A simple parameter often used in cold spray is FR given in Eq. 4. FR is a basic measure of the extent of deformation experienced by a powder particle at impact. Here, for all particles deposited by LIPIT, a linear relation between FR and velocity is identified (Fig. 4). The equivalent size of the powder particle and substrate surface morphology, also indicated in Fig. 4, have a minor influence on the FR.

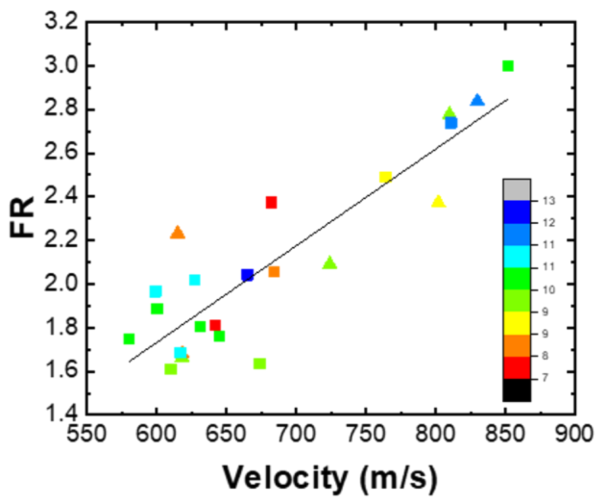


**Fig. 4.** Relationship between FR and velocity for Ti powder particles deposited by LIPIT. A color scheme is used to represent the equivalent powder diameter D (in μm) of each bonded particle. Powder particles that have impacted flat portions of the substrate are identified by triangular symbols while powder particles that impacted granular portions are identified by square symbols.

In the LIPIT system, velocity, particle size and substrate surface morphology are the main independent variables, provided that the materials used are not altered, and particle temperature is fixed at room temperature. From our finding in Fig. 4, that FR is strongly dependent on impact velocity with no major influences from diameter or substrate surface morphology, FR could in principle be used to back out a reasonable estimate of the 'effective velocity' of individual powder particles deposited by cold spray, albeit with a mismatch in temperature between those processes, which is expected to be significant. We examine this concept in the following.

Table I includes the average in-flight velocity of powder particles for the five spray conditions used, as measured by the Coldspraymeter in addition to the numerically simulated temperature of the powder at the exit of the nozzle. For each average in-flight velocity, the average FR of splats is measured. The linear dependence between FR and velocity is shown in Fig. 5 and is consistent with the trend identified by LIPIT testing (Fig. 4) and also with numerous observations of FR increasing with particle velocity in the cold spray literature [1, 30, 39, 48]. For a given velocity, FR measured on cold sprayed splats is consistently larger than FR measured on LIPIT splats. This is due to the different particle sizes used and the differences in temperature of the impacting particles. Interestingly, though, depositing particles at similar velocities using different gas temperatures, by cold spray, does not result in significant differences in FR. For example, FR of particles deposited by using the long nozzle at spray conditions of 4.9 MPa and 450°C are similar to the FR of particles deposited using the standard nozzle at 4.0 MPa and 800°C. These two spray conditions have very similar average particle velocities with very different particle temperatures. Thus, for these experiments, in terms of cold spray, particle velocity can be directly correlated to FR in the same way as for LIPIT. The difference of 295°C in particle temperature and the potential bow shock effect from an increase in pressure at the substrate surface does not appear to have a significant impact on FR.

**Table I**

Experimental average particle velocity and modeled particle temperature for powder particles deposited by cold spray under different spray conditions

| Nozzle Geometry | Spray Conditions | Experimental Average Particle Velocity (m/s) | Modeled Particle Temperature at Exit of Nozzle (°C) |
|---|---|---|---|
| Standard Nozzle | 4.0 MPa, 400°C | 491 ± 127 | 183 |
| Standard Nozzle | 4.0 MPa, 600°C | 543 ± 133 | 322 |
| Standard Nozzle | 4.0 MPa, 800°C | 692 ± 133 | 459 |
| Long Nozzle | 4.9 MPa, 450°C | 695 ± 136 | 166 |
| Long Nozzle | 4.9 MPa, 800°C | 768 ± 151 | 343 |

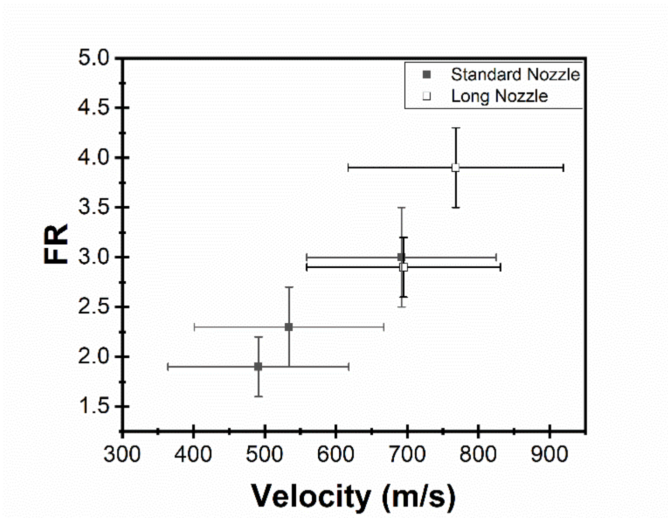


**Fig. 5.** The dependence of FR with velocity for powder particles deposited by cold spray.

## 3.3. Splat adhesion testing

### 3.3.1. Effect of substrate surface morphology

Particles impacting at similar velocities have relatively similar splat morphologies (Fig. 6 (a) and (c)), but their bond strength, as measured by splat adhesion testing, can vary significantly. The difference in adhesion strength can be understood by post-mortem observations of failed interfaces. Certain splats landed on the fine granular portion of the substrate, while others landed on the comparatively flat portions. The few splats that landed on smoother portions of the substrates show fine traces of Ti remaining on the substrate and weak bonding (Fig. 6 (b)). Conversely, particles landing on granular portions of the substrate show more retention of Ti between grains following splat adhesion testing (Fig. 6 (d)). More retention is associated with higher bond strengths as it is indicative of a continuous interface where Ti has penetrated within the valleys of the surface roughness. The interface bond strength is stronger than the cohesion strength of the Ti. A portion of Ti remaining between grains and having adapted to the surface morphology of the substrate has been identified by an arrow in Fig. 6 (d).

The granular surface morphology results in several points of contact with the impacting particles. By reducing the contact area, small high stress regions are formed [49]. This improves deformation and also allows the particles to penetrate within pores upon impact. Post observations of the failed interfaces indicate that mechanical bonding significantly contributes to adhesion. The splat adhesion test tip applies a tangential load on the splat. The splats which are strongly mechanically bonded are sheared rather than pulled out from within the grains as this is the weakest point in the system.

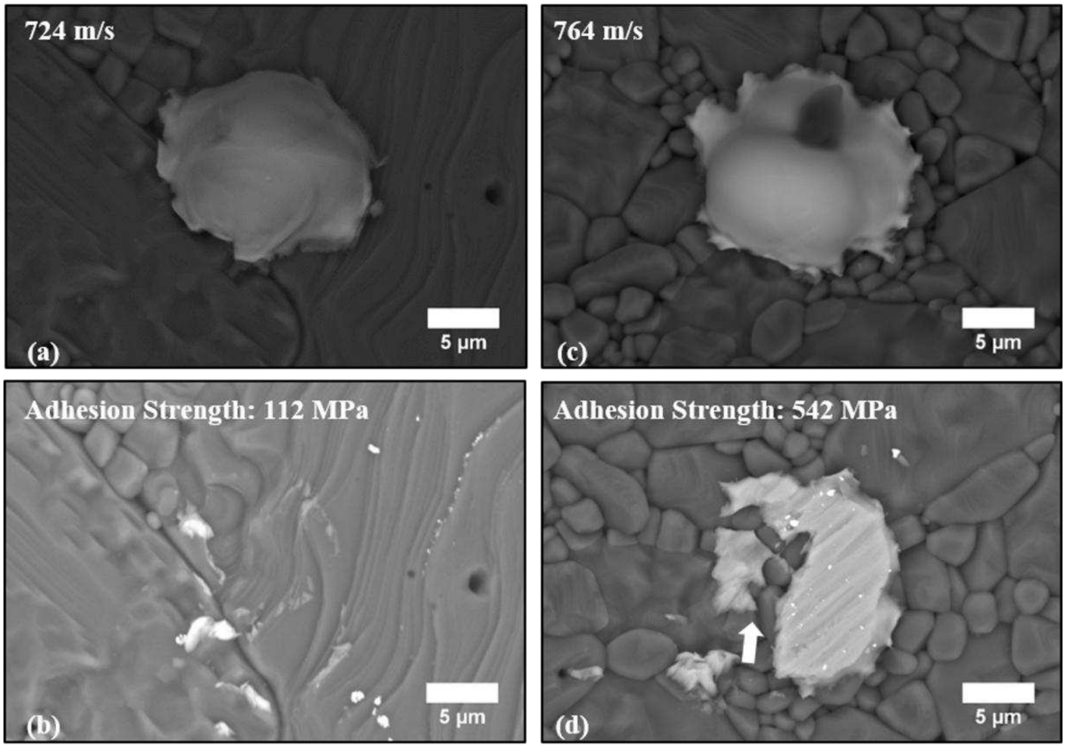


**Fig. 6.** A single Ti splat accelerated by LIPIT towards the $Al_2O_3$ substrate at a velocity of (a) 724 m/s (b) 764 m/s is shown. The Ti splat showed in (a/b) was removed by splat adhesion testing. The failed interface is shown (b/d).

Tested splats deposited by cold spray have a larger diameter than those deposited by LIPIT. Due to local heterogeneity of the substrate surface morphology, splats with a larger diameter are more likely to impact portions of the substrate with a combination of flat and granular portions of the substrate. In Fig. 7, post-test characterization of the failed interface shows about half of the splat on a granular portion of the substrate and the other half on a flat portion. Similar to what was observed for LIPIT splats, there is more retention in the granular portion of the substrate.

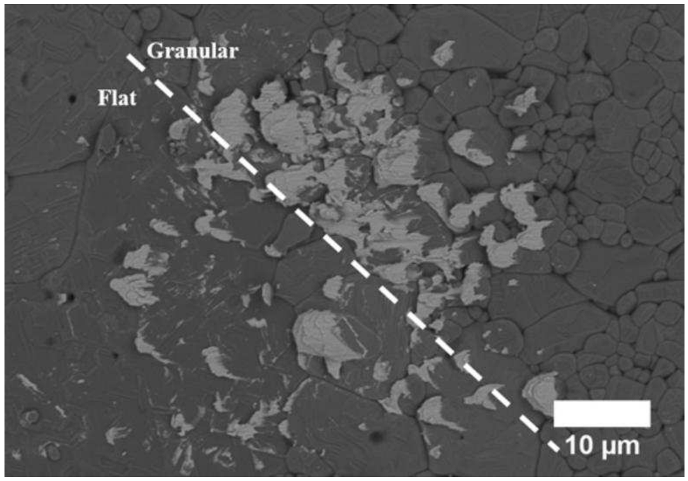


**Fig. 7.** Post-test characterization of a single splat deposited by cold spray. The splat landed on both a granular and flat part of the substrate. More Ti remained on the substrate in the region that is more granular.

The above observations correlate residual titanium penetrated into the surface porosity with adhesion strength. A quantitative analysis is required to further confirm the trend for LIPIT splats (Fig. 8). The area represented by Ti remaining in failed interfaces was analysed through color thresholding on SEM images, and converted to an area fraction over the projected splat area (Fig. 8 (d)). The amount of Ti remaining on the substrate is thus representative of the portions of the particles that are strongly bonded mechanically. The increase in adhesion strength with amount of Ti remaining in the failed interface is observable for both the smooth and granular parts of the substrate surface, and is in line with previous similar observations for $Ti/Al_2O_3$ interfaces created by cold spray [38]. Hence, the present results for $Ti/Al_2O_3$ interfaces emphasize the importance of mechanical bonding on adhesion strength.

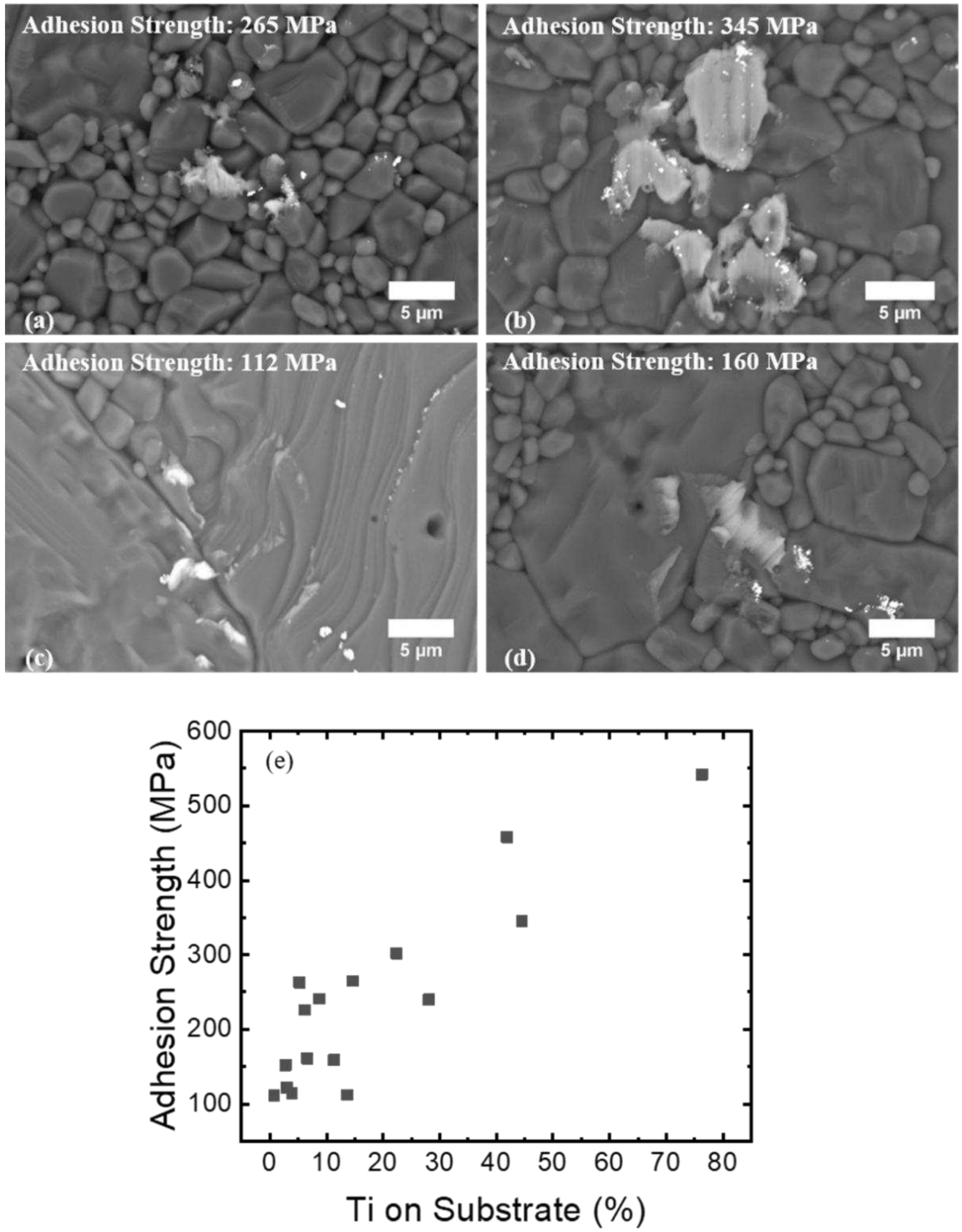


**Fig. 8.** Failed interfaces following splat adhesion tests at various velocities for Ti powder particles deposited on $Al_2O_3$ by LIPIT on (a, b) a granular part of the substrate and (c, d) a flat part of the substrate. (e) The area fraction of Ti remaining in the failed interface with respect to adhesion strength.

### 3.3.2. Flattening Ratio and Adhesion Strength

FR is a characteristic to individual cold spray splats and is linked to their impact velocity per results shown in Fig. 5. Therefore, while there is significant scatter in inflight particle velocity at each spray condition (Table I), the relative impact velocity of individual cold spray splats can be approximated by FR to understand its effect on adhesion strength. For this analysis, FR values are grouped into intervals of 0.5 to reduce point to point scatter and more accurately investigate broader trends.

It was confirmed that, at similar particle velocities, FR is not strongly influenced by variations in gas temperature but it is also deemed necessary to validate that variations in gas temperature do not significantly affect adhesion strength measurements. Adhesion strength measurements for splats deposited at 4.0 MPa and 800°C using the standard nozzle are compared to values obtained for splats deposited at 4.9 MPa and 450°C using the long nozzle as these represent identical in-flight velocity ranges with different gas temperatures (Fig. 9). Given high variations in particle velocity for the selected cold spray conditions (Table I), FR varies from 2.5 to 3.5. In both ranges of FR (2.5-3.0 and 3.0-3.5), a t-test shows no significant differences in the average adhesion strength especially considering that the adhesion strength is also influenced by local substrate surface morphology as previously discussed.

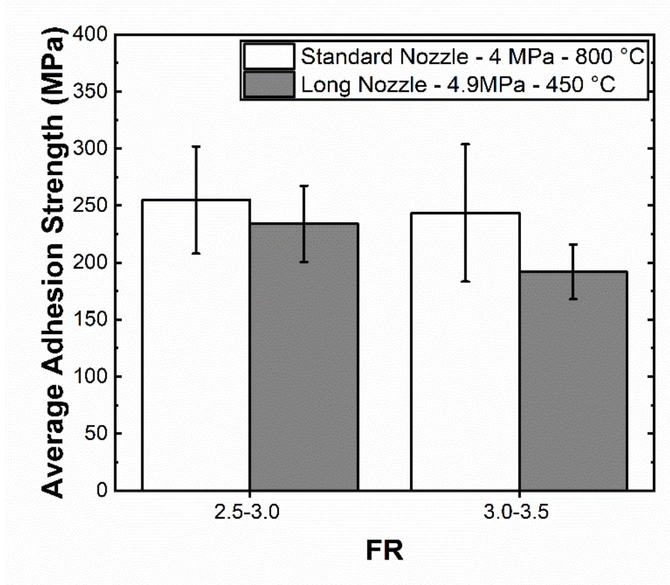


**Fig. 9.** Average splat adhesion strength measurements for splats deposited using the long nozzle at 4.9 MPa and 450°C (695 ± 136 m/s) and standard nozzle at 4.0 MPa and 800°C (692 ± 133 m/s) in two FR ranges of 2.5-3.0 and 3.0-3.5.

Given these results, splats from all spray conditions are taken as one dataset and are categorized based on their FR. Fig. 10 shows the average splat adhesion strengths at various FRs. The splat adhesion strength for Ti splats on an $Al_2O_3$ substrate decreases with an increase in FR, which is directly proportional to impact velocity. It should be noted that the decreasing trend for adhesion strength with an increase in FR is statistically significant as validated by a t-test.

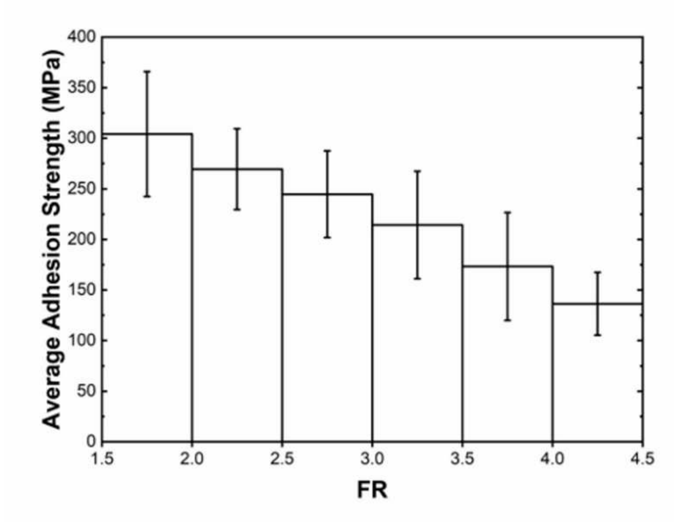


**Fig. 10.** Average splat adhesion strength measurements with respect to FR showing a decreasing trend for cold sprayed particles.

In section 3.3.1, the Ti remaining on the substrate is shown to be related to adhesion strength and is highly influenced by changes in substrate surface morphology. Since the percentage of Ti remaining on the substrate is measured following adhesion strength measurements, it is verified that this percentage of Ti is not influenced by velocity and is in fact an independent variable related to substrate surface morphology (Fig. 11). Despite the decreasing trend observed between adhesion strength and FR, there is no distinguishable trend between the amount of Ti on the substrate and FR between 1.5 and 3.5. For FR between 3.5 and 4.5, there is a weak decrease in the percent Ti remaining on the substrate, but a t-test confirmed that this decrease is not statistically significant.

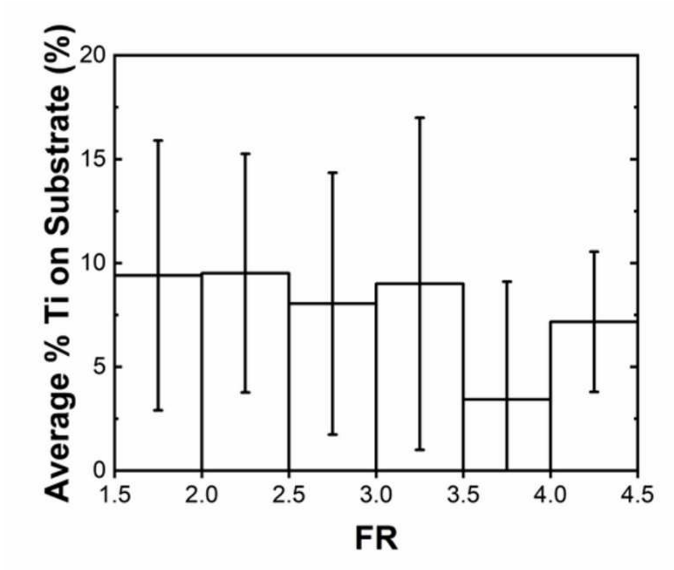


**Fig. 11.** Percent bonded of Ti powder particles in post-test characterization of splats deposited by cold spray plotted with respect to FR.

FR values between 3.5 and 4.5 are mainly results of splats deposited at 4.9 MPa and 800 ºC using the long nozzle. The slight decrease in percentage of Ti remaining on the substrate is associated to fracturing of the ceramic beneath the splat in post-test characterization for many splats deposited under these spray conditions (Fig. 12). While fracturing is observed for some particles deposited at lower velocities, it occurred so infrequently that it is not considered a predominant failure mechanism. Given that the splat adhesion test tip applies a tangential force on the splat, it is unlikely that fracturing occurs due to testing itself. Instead, it is likely that, at this spray condition, the ceramic fractures due to impact of the splat at the high velocity around 768 ± 151 m/s. No fracturing has been observed for splats deposited at similar velocities by LIPIT, however, the particles are smaller than those tested in cold spray. At the same velocities and for the same materials, smaller particles have lower kinetic energy than larger particles, and may thus require higher velocities yet to induce fracture of the substrate.

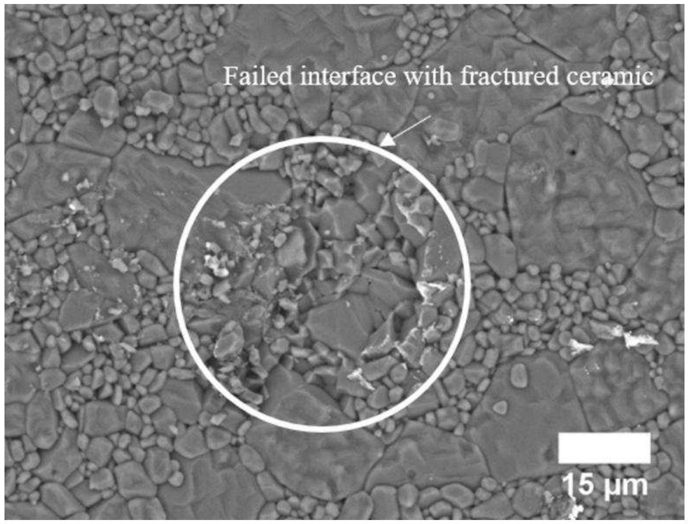


**Fig. 12.** Post-test characterization of splats deposited using the long nozzle at 4.9 MPa and 800ºC. That is, splat deposited at the highest velocity in this study. The failed interface shows fracturing of the ceramic.

## 4. Discussion

### 4.1. Ti-Particle Deposition

To identify factors influencing deposition in cold spray, the analysis of single splats is commonly used and often referred to as a wipe test [1, 8, 19, 41]. However, given the large range in particle velocity for individual spray conditions, as notable in Table I, a drawback for wipe tests remains the inability to identify the precise deposition velocity of a single splat. By LIPIT, the deposition velocities of single splats are measured and can be used to identify the critical velocity and factors affecting deposition such as substrate morphology. From Fig. 3, the critical velocity was identified to be between 580 – 620 m/s, beyond which most splats bond to the substrate. A single observation of particle rebound occurred at 750 m/s but this may be due to substrate fracture, similar to that observed for splats cold sprayed at high velocity (see Fig. 12). No prior work has identified the required critical velocity for this material system. While in cold spray the critical velocity is influenced by particle size [8] and gas temperature [28, 29], the range obtained here, by LIPIT, is a valid first approximation of critical velocity for a Ti/$Al_2O_3$ interface.

The LIPIT technique also allows for a comparison of FR with velocity identifying a linear trend as expected. To achieve higher velocities in cold spray, options include increasing gas pressure, increasing gas temperature, changing the nozzle geometry or changing the gas type. Here, to achieve a wide range of velocities, the process gas conditions and the nozzle geometry are varied. This approach also has the benefit of using spray conditions with similar in-flight particle velocities at very different gas and particle temperatures. Using the two nozzle geometries, a gas temperature difference of 350°C could be used while maintaining a similar velocity. This gas temperature difference is associated with an approximate difference in particle temperature of 295°C. Comparing first cold sprayed splats to LIPIT splats, thermal softening due to particle impact temperature results in additional powder deformation, which is measurable by FR. For similar velocities, cold sprayed splats generally had higher FR than LIPIT splats. However, when comparing results for cold sprayed splats deposited within the range of temperatures used, between 400 - 800°C, the effect of temperature on the FR appears to be negligible. That is, while increasing gas temperature for either nozzle results in an increase in particle velocity (see Table I), conditions where the in-flight velocity was the same but with drastically different temperatures resulted in similar FR (Fig. 5) and adhesion strength (Fig. 9). Another important observation is the maintained proportionality between FR and particle velocity when using the long nozzle in comparison to the standard nozzle (Fig. 5). This occurs despite a disproportionate increase in temperature and further confirms that the relationship between FR and particle velocity is likely minimally influenced by the effect of the gas temperature for the Ti/$Al_2O_3$ interface.

### 4.2. Bonding Mechanism and Adhesion Strength

For proper interpretation of splat adhesion test results, analysis of the failed interfaces is essential [38]. In the Ti/$Al_2O_3$ interface, the material remaining on the substrate from the splat is clearly identifiable and its footprint can be used to determine factors contributing to adhesion [38]. As previously discussed by Imbriglio et al. [38], splat failure under tangential load occurs through the weakest part of the interface. Low adhesion strengths are typically correlated with interface failure and very little Ti remaining on the substrate. High adhesion strength results typically show a significant amount of Ti on the substrate as the interface adhesion strength is higher than cohesion in the splat. The contribution of sheared Ti in the failure mechanism is particularly important when Ti has infiltrated surface porosity as the interface consists of both $Al_2O_3$ and Ti [38]. Similar to previous results for this interface [38], the adhesion strengths reported here for many splats, are considered to be relatively high. Near the interface, grain refinement is characteristic of cold spray Ti splats due to extreme plastic deformation at impact [50-52]. Thus, the mechanical properties near the interfaces are different than the original Ti powder or bulk Ti [50]. When failure occurs, through the Ti, near the interface, grain refinement may contribute to the high adhesion strength measurements [38].

Post-test characterization of failed interfaces and adhesion strength measurements of splats deposited by LIPIT demonstrate the importance of mechanical clamping in the formation of a bond on a rough substrate. These results are consistent with some prior observations of failed interfaces of cold sprayed splats showing that the infiltration of Ti into the surface porosity of as-received polycrystalline $Al_2O_3$ contributes to adhesion [38]. However, it has also been previously reported that metal powder particles can bond to atomically smooth ceramic substrates by a chemical bond [15, 17, 19, 22, 25]. Imbriglio et al. suggested that chemical bonding is likely the primary bonding mechanism on polished $Al_2O_3$ surfaces [38]. In such situations the specific state of the surface apparently becomes important: particles impacting on comparatively flat portions of as-received substrates show quite different behavior from well-polished surfaces of the same material. Whereas polished surfaces show chemical adhesion rings [38], flat portions of as-received substrates are still nanoscopically rough compared to the polished surfaces and do not. Post-test characterization of failed interfaces on flat portions of the substrate show very little Ti retention on the substrate but adhesion strength measurements still approach ≈ 100 MPa. Therefore, while chemical adhesion rings are not observed, chemico-physical factors may still contribute to the formation of a bond. The possibility of having both mechanical and chemico-physical factors influencing adhesion has previously been discussed by Wüstefeild et al. who observed local heteroepitaxy between Al coatings deposited on polycrystalline AlN substrates and infiltration of Al into the surface porosity of the AlN substrate [22]. These chemico-physical factors may also play a role in high adhesion strength measurements recorded, in this work, for rough portions of the substrate. The interfacial adhesion strength is a result of both crack propagation through chemically bonded portions of the splats and shearing of Ti. Splats bonding to mostly flat portions of the substrate have a smaller contribution from sheared Ti resulting in their lower adhesion strength.

The adhesion strength is also observed to decrease with an increase in FR. An increase in FR results in an increase in the projected splat area, typically expected to form a stronger bond. Yet, the opposite is observed. One factor that is shown to influence adhesion strength is fracture of the ceramic (Fig. 12). However, fracture of the ceramic during impact is not believed to be the sole contributing factor to the decrease in adhesion strength of single splats with increasing FR.

FR was shown to be related to the deposition velocity. As the velocity is increased adhesion and rebound energies act as competing effects. If the rebound energy becomes greater than the adhesion energy at high velocities, particles will not adhere to the substrate. There is an optimal range for deposition bounded by a minimum and maximum critical velocity [53]. While the effect of velocity on adhesion in metal/ceramic interfaces created by cold spray has not been examined in the literature, some authors have attempted to understand this effect in metal/metal interfaces. Wu et al. showed experimentally that as the velocity is increased for deposition of Al-Si powder onto mild steel, the ratio between bonded particles to the total amount of deposited particles reaches a maximum value and then decreases significantly as the velocity is increased due to this rebound phenomenon [53]. In a soft particle/hard substrate interface, the recoverable strain energy increases considerably at higher velocities causing the rebound phenomenon [54]. Within the range where deposition is possible, the ratio between rebound energy and adhesion energy reaches a minimum and then tends to increase. This trend is more pronounced in soft powder (Al)/ hard substrate (Mild Steel) interfaces [55]. The rebound phenomenon may cause nanoscopic porosity at the interface rendering lower adhesion strength. In addition to the rebound phenomenon, there is a maximum deposition velocity that, when reached, causes erosion of the interfacing materials [8, 10, 37, 41]. The maximum impact velocity is often referred to as the erosion velocity and defines the maximum boundary of the window of sprayability [8]. The window of sprayability is known to be reduced when using brittle materials [8, 18]. Here, a decrease in adhesion strength is attributed to competing rebound and adhesion energies in addition to fracture of the ceramic at very high velocities. Fracture of the ceramic when depositing powder at 4.9 MPa and 800°C is indicative of the early limit of the window of sprayability. Within the deposition conditions used in this study, only a decrease in adhesion strength was observed. Per LIPIT results, below approximately 580 m/s particles will not adhere. For cold spray, the splats deposited using the lowest gas temperature with the standard nozzle have an impact velocity relatively close to this critical velocity.

## 5. Conclusion

The influencing parameters on the formation of a bond in a metal/ceramic interface by high speed impact are still unclear in the literature. To better understand some influencing parameters, Ti particles are deposited by LIPIT and cold spray on polycrystalline $Al_2O_3$ substrates. Specific parameters of interest include identifying critical velocity for this material system, understanding the effect of substrate local heterogeneity when using sintered ceramic substrates and the effect of velocity on adhesion strength. For the first time, the critical velocity for deposition of Ti onto $Al_2O_3$ by high speed impact is identified to be between 580-620 m/s by use of the LIPIT system.

The splat adhesion test is used to measure the adhesion of individual splats. Substrate morphology and deposition velocity of individual splats are identified as influencing parameters on adhesion strength. By knowing the deposition velocity of individual splats when using LIPIT, the effect of substrate surface morphology is isolated from the velocity effect. Splats landing on comparatively smooth portions of the substrates have significantly lower bond strengths than those landing on rough portions of the substrates. The influence of substrate surface morphology on bond strength is important as mechanical bonding is found to contribute significantly to adhesion in this $Ti/Al_2O_3$ interface. Individual splats also have a characteristic FR related to the particle velocity at impact. The effect of particle velocity on FR is studied for splats deposited by both LIPIT and cold spray. The cold sprayed splats show that adhesion strength tends to decrease with an increase in FR despite the dependence between adhesion strength and substrate surface morphology. This effect can be associated with fracture of the ceramic at very high velocities and competing effects between adhesion and rebound energies.

**Acknowledgment**

RRC and SII acknowledge the assistance of Dr. Phuong Vo and Jean-Francois Alarie at the National Research Council Canada for technical support with the cold spray equipment and Drs. Thomas Schmitt and Jolanta Sapieha from Polytechnique Montreal for technical support and access to the scratch tester. This work was supported by the Natural Science and Engineering Research Council (NSERC) Strategic Grants Program.

MHG and CAS acknowledge support from the US Army Research Laboratory, Contract: W911NF-15-2-0034, "Development of Additive Manufacturing and Advanced Materials Processing for the DOD". DV and KAN acknowledge support from the U. S. Army Research Office through the Institute for Soldier Nanotechnologies, under Cooperative Agreement Numbers W911NF-13-D-0001 and W911NF-18-2-0048 as well as support for equipment through the Office of Naval Research DURIP Grant No. N00014-13-1-0676.

**References:**


[1] H. Assadi, F. Gärtner, T. Stoltenhoff, H. Kreye, Bonding mechanism in cold gas spraying, Acta Mater., 51 (2003) 4379-4394. https://doi.org/10.1016/S1359-6454(03)00274-X.

[2] M. Grujicic, J.R. Saylor, D.E. Beasley, W.S. DeRosset, D. Helfritch, Computational analysis of the interfacial bonding between feed-powder particles and the substrate in the cold-gas dynamic-spray process, Appl. Surf. Sci., 219 (2003) 211-227. https://doi.org/10.1016/S0169-4332(03)00643-3.

[3] M. Grujicic, C.L. Zhao, W.S. De Rosset, D. Helfritch, Adiabatic shear instability based mechanism for particles/substrate bonding in the cold-gas dynamic-spray process, Mater. Des., 25 (2004) 681-688. https://doi.org/10.1016/j.matdes.2004.03.008.

[4] T. Hussain, D.G. McCartney, P.H. Shipway, D. Zhang, Bonding mechanisms in cold spraying: The contributions of metallurgical and mechanical components, J. Therm. Spray Technol., 18 (2009) 364-379. https://doi.org/10.1007/s11666-009-9298-1.

[5] M. Hassani-Gangaraj, D. Veysset, V.K. Champagne, K.A. Nelson, C.A. Schuh, Adiabatic shear instability is not necessary for adhesion in cold spray, Acta Mater., 158 (2018) 430-439. https://doi.org/10.1016/j.actamat.2018.07.065.

[6] S. Kumar, G. Bae, C. Lee, Influence of substrate roughness on bonding mechanism in cold spray, Surf. Coat. Technol., 304 (2016) 592-605. https://doi.org/10.1016/j.surfcoat.2016.07.082.

[7] T. Stoltenhoff, H. Kreye, H.J. Richter, An analysis of the cold spray process and its coatings, J. Therm. Spray Technol., 11 (2002) 542-550. https://doi.org/10.1361/105996302770348682.

[8] T. Schmidt, F. Gärtner, H. Assadi, H. Kreye, Development of a generalized parameter window for cold spray deposition, Acta Mater., 54 (2006) 729-742. https://doi.org/10.1016/j.actamat.2005.10.005.

[9] M. Hassani-Gangaraj, D. Veysset, K.A. Nelson, C.A. Schuh, In-situ observations of single micro-particle impact bonding, Scr. Mater., 145 (2018) 9-13. https://doi.org/10.1016/j.scriptamat.2017.09.042.

[10] H. Assadi, T. Schmidt, H. Richter, J.O. Kliemann, K. Binder, F. Gärtner, T. Klassen, H. Kreye, On parameter selection in cold spraying, J. Therm. Spray Technol., 20 (2011) 1161-1176. https://doi.org/10.1007/s11666-011-9662-9.

[11] H. Assadi, H. Kreye, F. Gärtner, T. Klassen, Cold spraying - a materials perspective, Acta Mater., 116 (2016) 382-407. https://doi.org/10.1016/j.actamat.2016.06.034.

[12] M.R. Rokni, S.R. Nutt, C.A. Widener, V.K. Champagne, R.H. Hrabe, Review of relationship between particle deformation, coating microstructure, and properties in high-pressure cold Spray, J. Therm. Spray Technol., 26 (2017) 1308-1355. https://doi.org/10.1007/s11666-017-0575-0.

[13] R.R. Chromik, S.A. Alidokht, J.M. Shockley, Y. Zhang, Tribological coatings prepared by cold spray, in: P. Cavaliere (Ed.) Cold-spray coatings: Recent trends and future perspectives, Springer International Publishing, Cham, Switzerland, 2018, pp. 321-348.

[14] R. Drehmann, T. Grund, T. Lampke, B. Wielage, K. Manygoats, T. Schucknecht, D. Rafaja, Splat formation and adhesion mechanisms of cold gas-sprayed Al coatings on $Al_2O_3$ substrates, J. Therm. Spray Technol., 23 (2014) 68-75. https://doi.org/10.1007/s11666-013-9966-z.

[15] R. Drehmann, T. Grund, T. Lampke, B. Wielage, K. Manygoats, T. Schucknecht, D. Rafaja, Interface characterization and bonding mechanisms of cold gas-sprayed Al coatings on ceramic substrates, J. Therm. Spray Technol., 24 (2015) 92-99. https://doi.org/10.1007/s11666-014-0189-8.

[16] R. Drehmann, T. Grund, T. Lampke, B. Wielage, C. Wüstefeld, M. Motylenko, D. Rafaja, Essential factors influencing the bonding strength of cold-sprayed aluminum coatings on ceramic substrates, J. Therm. Spray Technol., 27 (2018) 446-455. https://doi.org/10.1007/s11666-018-0688-0.

[17] D. Rafaja, T. Schucknecht, V. Klemm, A. Paul, H. Berek, Microstructural characterisation of titanium coatings deposited using cold gas spraying on $Al_2O_3$ substrates, Surf. Coat. Technol., 203 (2009) 3206-3213. https://doi.org/10.1016/j.surfcoat.2009.03.054.

[18] K.-R. Donner, F. Gaertner, T. Klassen, Metallization of thin $Al_2O_3$ layers in power electronics using cold gas spraying, J. Therm. Spray Technol., 20 (2011) 299-306. https://doi.org/10.1007/s11666-010-9573-1.

[19] K.R. Ernst, J. Braeutigam, F. Gaertner, T. Klassen, Effect of substrate temperature on cold-gas-sprayed coatings on ceramic substrates, J. Therm. Spray Technol., 22 (2013) 422-432. https://doi.org/10.1007/s11666-012-9871-x.

[20] K.H. Ko, J.O. Choi, H. Lee, The interfacial restructuring to amorphous: A new adhesion mechanism of cold-sprayed coatings, Mater. Lett., 175 (2016) 13-15. https://doi.org/10.1016/j.matlet.2016.03.132.

[21] B. Wielage, T. Grund, C. Rupprecht, S. Kuemmel, New method for producing power electronic circuit boards by cold-gas spraying and investigation of adhesion mechanisms, Surf. Coat. Technol., 205 (2010) 1115-1118. https://doi.org/10.1016/j.surfcoat.2010.06.020.

[22] C. Wüstefeld, D. Rafaja, M. Motylenko, C. Ullrich, R. Drehmann, T. Grund, T. Lampke, B. Wielage, Local heteroepitaxy as an adhesion mechanism in aluminium coatings cold gas sprayed on AlN substrates, Acta Mater., 128 (2017) 418-427. https://doi.org/10.1016/j.actamat.2017.02.021.

[23] A. Moridi, S.M. Hassani-Gangaraj, M. Guagliano, M. Dao, Cold spray coating: Review of material systems and future perspectives, Surf. Eng., 30 (2014) 369-395. https://doi.org/10.1179/1743294414Y.0000000270.

[24] A. Viscusi, A. Astarita, R.D. Gatta, F. Rubino, A perspective review on the bonding mechanisms in cold gas dynamic spray, Surf. Eng., (2018) 1-29. https://doi.org/10.1080/02670844.2018.1551768.

[25] P.C. King, S. Zahiri, M. Jahedi, J. Friend, Aluminium coating of lead zirconate titanate - a study of cold spray variables, Surf. Coat. Technol., 205 (2010) 2016-2022. http://dx.doi.org/10.1016/j.surfcoat.2010.08.084.

[26] P.C. King, S.H. Zahiri, M. Jahedi, Focused ion beam micro-dissection of cold-sprayed particles, Acta Mater., 56 (2008) 5617-5626. https://doi.org/10.1016/j.actamat.2008.07.034.

[27] J. Villafuerte, Modern cold spray : Materials, process, and applications, Springer, Windsor, Ontario, Canada, 2015.

[28] W. Wong, E. Irissou, A.N. Ryabinin, J.-G. Legoux, S. Yue, Influence of helium and nitrogen gases on the properties of cold gas dynamic sprayed pure titanium coatings, J. Therm. Spray Technol., 20 (2011) 213-226. https://doi.org/10.1007/s11666-010-9568-y.

[29] J. Lee, S. Shin, H. Kim, C. Lee, Effect of gas temperature on critical velocity and deposition characteristics in kinetic spraying, Appl. Surf. Sci., 253 (2007) 3512-3520. https://doi.org/10.1016/j.apsusc.2006.07.061.

[30] D. Goldbaum, J.M. Shockley, R.R. Chromik, A. Rezaeian, S. Yue, J.G. Legoux, E. Irissou, The effect of deposition conditions on adhesion strength of Ti and Ti6Al4V cold spray splats, J. Therm. Spray Technol., 21 (2012) 288-303. https://doi.org/10.1007/s11666-011-9720-3.

[31] J. Wu, H. Fang, S. Yoon, H. Kim, C. Lee, Measurement of particle velocity and characterization of deposition in aluminum alloy kinetic spraying process, Appl. Surf. Sci., 252 (2005) 1368-1377. https://doi.org/10.1016/j.apsusc.2005.02.108.

[32] J.H. Lee, P.E. Loya, J. Lou, E.L. Thomas, Dynamic mechanical behavior of multilayer graphene via supersonic projectile penetration, Science, 346 (2014) 1092-1096. https://doi.org/10.1126/science.1258544.

[33] J.-H. Lee, D. Veysset, J.P. Singer, M. Retsch, G. Saini, T. Pezeril, K.A. Nelson, E.L. Thomas, 2012. High strain rate deformation of layered nanocomposites, Nat. Commun. 3, 1164 (2012). https://doi.org/10.1038/ncomms2166.

[34] D. Veysset, A.J. Hsieh, S.E. Kooi, K.A. Nelson, Molecular influence in high-strain-rate microparticle impact response of poly (urethane urea) elastomers, Polymer, 123 (2017) 30-38. https://doi.org/10.1016/j.polymer.2017.06.071.

[35] D. Veysset, A.J. Hsieh, S. Kooi, A.A. Maznev, K.A. Masser, K.A. Nelson, 2016. Dynamics of supersonic microparticle impact on elastomers revealed by real–time multi–frame imaging, Sci. Rep. 6, 25577. https://doi.org/10.1038/srep25577.

[36] M. Hassani-Gangaraj, D. Veysset, K.A. Nelson, C.A. Schuh, 2017. Melting can hinder impact-induced adhesion, Phys. Rev. Lett. 119, 175701. https://doi.org/10.1103/PhysRevLett.119.175701.

[37] M. Hassani-Gangaraj, D. Veysset, K.A. Nelson, C.A. Schuh, 2018. Melt-driven erosion in microparticle impact, Nat. Commun. 9, 5077(2018) . https://doi.org/10.1038/s41467-018-07509-y.

[38] S.I. Imbriglio, N. Brodusch, M. Aghasibeig, R. Gauvin, R.R. Chromik, Influence of substrate characteristics on single Ti splat bonding to ceramic substrates by cold spray, J. Therm. Spray Technol., 27 (2018) 1011-1024. https://doi.org/10.1007/s11666-018-0743-x.

[39] R.R. Chromik, D. Goldbaum, J.M. Shockley, S. Yue, E. Irissou, J.G. Legoux, N.X. Randall, Modified ball bond shear test for determination of adhesion strength of cold spray splats, Surf. Coat. Technol, 205 (2010) 1409-1414. https://doi.org/10.1016/j.surfcoat.2010.07.037.

[40] R. Huang, H. Fukanuma, Study of the influence of particle velocity on adhesive strength of cold spray deposits, J. Therm. Spray Technol., 21 (2012) 541-549. https://doi.org/10.1007/s11666-011-9707-0.

[41] T. Schmidt, H. Assadi, F. Gärtner, H. Richter, T. Stoltenhoff, H. Kreye, T. Klassen, From particle acceleration to impact and bonding in cold spraying, J. Therm. Spray Technol., 18 (2009) 794-808. https://doi.org/10.1007/s11666-009-9357-7.

[42] K. Sakaki, 7 - The influence of nozzle design in the cold spray process, in: V.K. Champagne (Ed.), The cold spray materials deposition process, Woodhead Publishing, 2007, pp. 117-126.

[43] K. Stephan, R. Krauss, A. Laesecke, Viscosity and thermal conductivity of nitrogen for a wide range of fluid states, J Phys Chem Ref Data, 16 (1987) 993-1023. https://doi.org/10.1063/1.555798.

[44] W.M. Rohsenow, J.P. Hartnett, Y.I. Cho, Handbook of heat transfer, 3rd ed., McGraw-Hill, New York, 1998.

[45] P.C. King, M. Jahedi, Relationship between particle size and deformation in the cold spray process, Appl. Surf. Sci., 256 (2010) 1735-1738. https://doi.org/10.1016/j.apsusc.2009.09.104.

[46] K. Kim, M. Watanabe, S. Kuroda, Thermal softening effect on the deposition efficiency and microstructure of warm sprayed metallic powder, Scr. Mater., 60 (2009) 710-713. https://doi.org/10.1016/j.scriptamat.2008.12.050.

[47] J.I. Goldstein, D.E. Newbury, P. Echlin, D.C. Joy, C.E. Lyman, E. Lifshin, L. Sawyer, J.R. Michael, Special topics in scanning electron microscopy, in: Scanning electron microscopy and x-ray microanalysis: Third edition, Springer US, Boston, MA, 2003, pp. 195-270.

[48] W.-Y. Li, H. Liao, C.-J. Li, G. Li, C. Coddet, X. Wang, On high velocity impact of micro-sized metallic particles in cold spraying, Appl. Surf. Sci., 253 (2006) 2852-2862. https://doi.org/10.1016/j.apsusc.2006.05.126.

[49] T. Hussain, Cold spraying of titanium: A review of bonding mechanisms, microstructure and properties, Key Eng. Mater., 533 (2012) 53-90. https://doi.org/10.4028/www.scientific.net/KEM.533.53.

[50] D. Goldbaum, R.R. Chromik, N. Brodusch, R. Gauvin, Microstructure and mechanical properties of Ti cold-spray splats determined by electron channeling contrast imaging and nanoindentation mapping, Microsc. Microanal., 21 (2015) 570-581. https://doi.org/10.1017/S1431927615000240.

[51] K. Kim, M. Watanabe, J. Kawakita, S. Kuroda, Grain refinement in a single titanium powder particle impacted at high velocity, Scr. Mater., 59 (2008) 768-771. https://doi.org/10.1016/j.scriptamat.2008.06.020.

[52] N. Cinca, J.M. Rebled, S. Estradé, F. Peiró, J. Fernández, J.M. Guilemany, Influence of the particle morphology on the cold gas spray deposition behaviour of titanium on aluminum light alloys, J. Alloys Compd., 554 (2013) 89-96. https://doi.org/10.1016/j.jallcom.2012.11.069.

[53] J. Wu, H. Fang, S. Yoon, H. Kim, C. Lee, The rebound phenomenon in kinetic spraying deposition, Scr. Mater., 54 (2006) 665-669. https://doi.org/10.1016/j.scriptamat.2005.10.028.

[54] G. Bae, Y. Xiong, S. Kumar, K. Kang, C. Lee, General aspects of interface bonding in kinetic sprayed coatings, Acta Mater., 56 (2008) 4858-4868. https://doi.org/10.1016/j.actamat.2008.06.003.

[55] A. Manap, H. Misran, O. Nooririnah, T. Okabe, K. Ogawa, Experimental and SPH study of cold spray impact between similar and dissimilar metals, Surf. Eng., 30 (2014) 335-341. https://doi.org/10.1179/1743294413Y.0000000237.

**Figure Captions**

**Fig. 1.** Surface morphology of the $Al_2O_3$ substrate. Portions of the substrate include large grains which make the substrate flatter than areas that include several small grains. Areas with small grains are identified as granular while areas with large grains are identified as flat.

**Fig. 2.** 12 snapshots captured by the high-frame-rate camera during LIPIT (cropped to emphasize regions of interest) with a 5-ns exposure time depicting the impact of a single micron-sized Ti particle impacting the $Al_2O_3$ substrate. (a) The powder particle impacts the substrate at a velocity of 455 m/s. Following impact, rebound occurs at 37 m/s. (b) The powder particle impacts the substrate at a velocity of 631 m/s and remains bonded to the substrate.

**Fig. 3.** Variation of COR with respect to impact velocity for Ti powder particles accelerated towards the $Al_2O_3$ substrate by LIPIT. Particles begin to bond to the substrate at 580 m/s. Bonded particles are depicted by blue markers on the null COR axis.

**Fig. 4.** Relationship between FR and velocity for Ti powder particles deposited by LIPIT. A color scheme is used to represent the equivalent powder diameter D (in μm) of each bonded particle. Powder particles that have impacted flat portions of the substrate are identified by triangular symbols while powder particles that impacted granular portions are identified by square symbols.

**Fig. 5.** The dependence of FR with velocity for powder particles deposited by cold spray.

**Fig. 6.** A single Ti splat accelerated by LIPIT towards the $Al_2O_3$ substrate at a velocity of (a) 724 m/s (b) 764 m/s is shown. The Ti splat showed in (a/b) was removed by splat adhesion testing. The failed interface is shown (b/d).

**Fig. 7.** Post-test characterization of a single splat deposited by cold spray. The splat landed on both a granular and flat part of the substrate. More Ti remained on the substrate in the region that is more granular.

**Fig. 8.** Failed interfaces following splat adhesion tests at various velocities for Ti powder particles deposited on $Al_2O_3$ by LIPIT on (a, b) a granular part of the substrate and (c, d) a flat part of the substrate. (e) The area fraction of Ti remaining in the failed interface with respect to adhesion strength.

**Fig. 9.** Average splat adhesion strength measurements for splats deposited using the long nozzle at 4.9 MPa and 450°C (695 ± 136 m/s) and standard nozzle at 4.0 MPa and 800°C (692 ± 133 m/s) in two FR ranges of 2.5-3.0 and 3.0-3.5.

**Fig. 10.** Average splat adhesion strength measurements with respect to FR showing a decreasing trend for cold sprayed particles.

**Fig. 11.** Percent bonded of Ti powder particles in post-test characterization of splats deposited by cold spray plotted with respect to FR.

**Fig. 12.** Post-test characterization of splats deposited using the long nozzle at 4.9 MPa and 800ºC. That is, splat deposited at the highest velocity in this study. The failed interface shows fracturing of the ceramic.

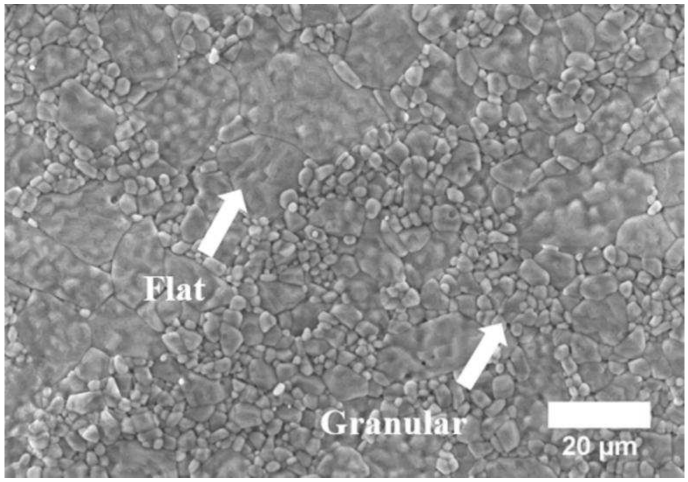


**Fig. 1.**

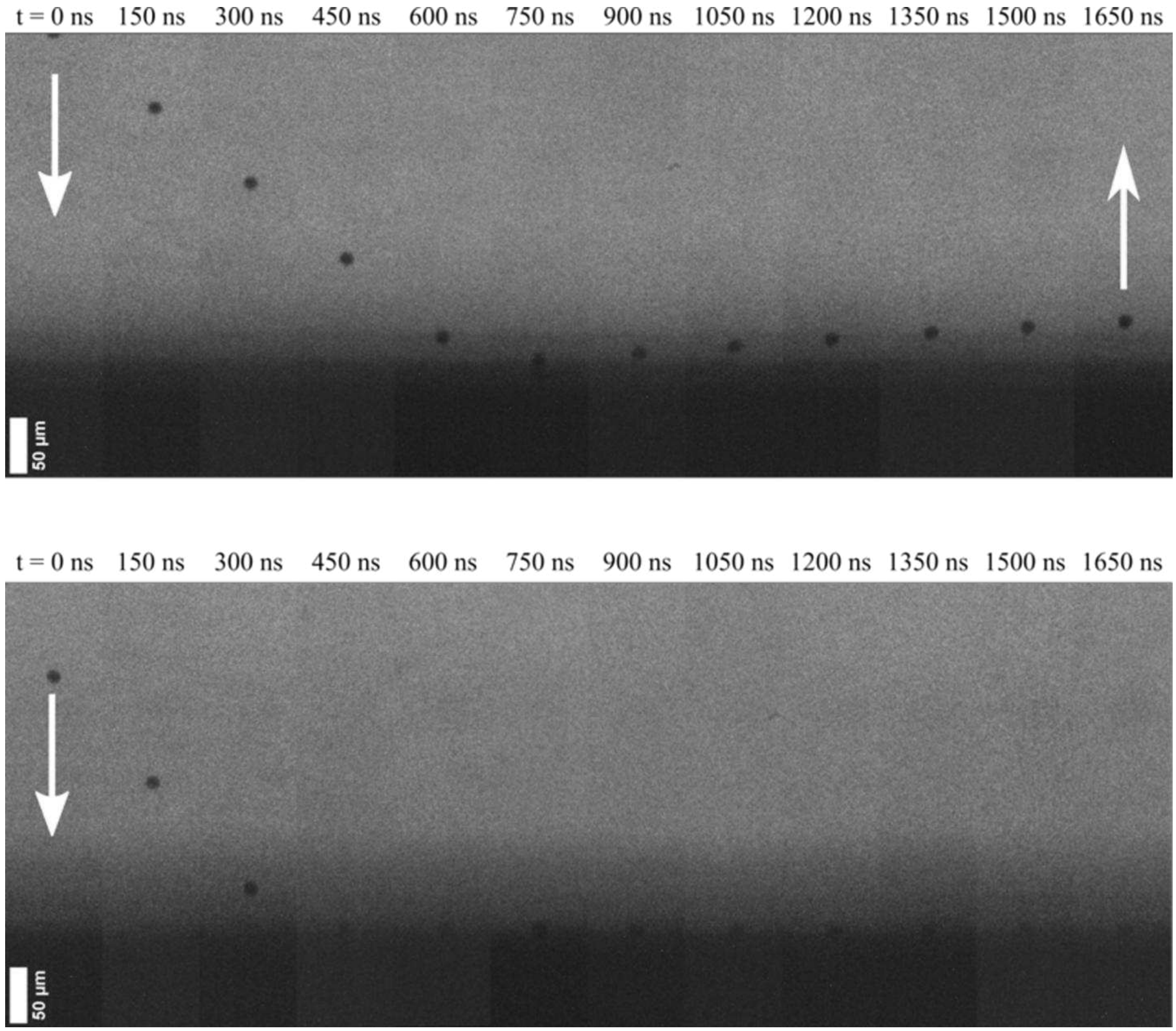
t = 0 ns 150 ns 300 ns 450 ns 600 ns 750 ns 900 ns 1050 ns 1200 ns 1350 ns 1500 ns 1650 ns
50 μm
t = 0 ns 150 ns 300 ns 450 ns 600 ns 750 ns 900 ns 1050 ns 1200 ns 1350 ns 1500 ns 1650 ns
50 μm

**Fig. 2.**

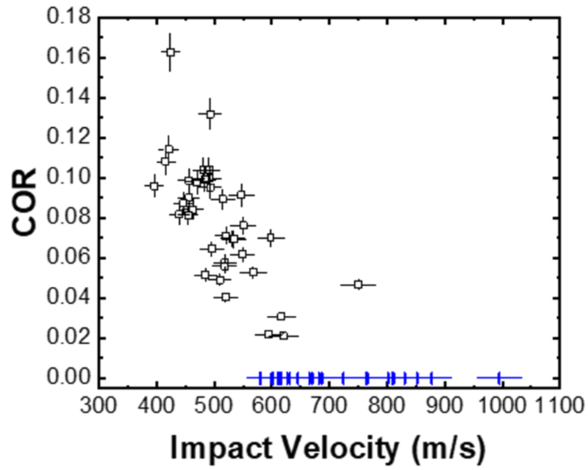
0.18
0.16
0.14
0.12
0.10
0.08
0.06
0.04
0.02
0.00
COR
300 400 500 600 700 800 900 1000 1100
Impact Velocity (m/s)

**Fig. 3.**

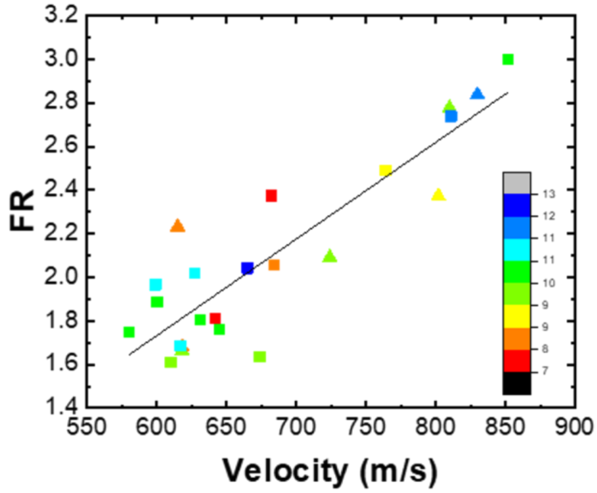
FR
Velocity (m/s)
3.2
3.0
2.8
2.6
2.4
2.2
2.0
1.8
1.6
1.4
550
600
650
700
750
800
850
900
13
12
11
11
10
9
9
8
7

**Fig. 4.**

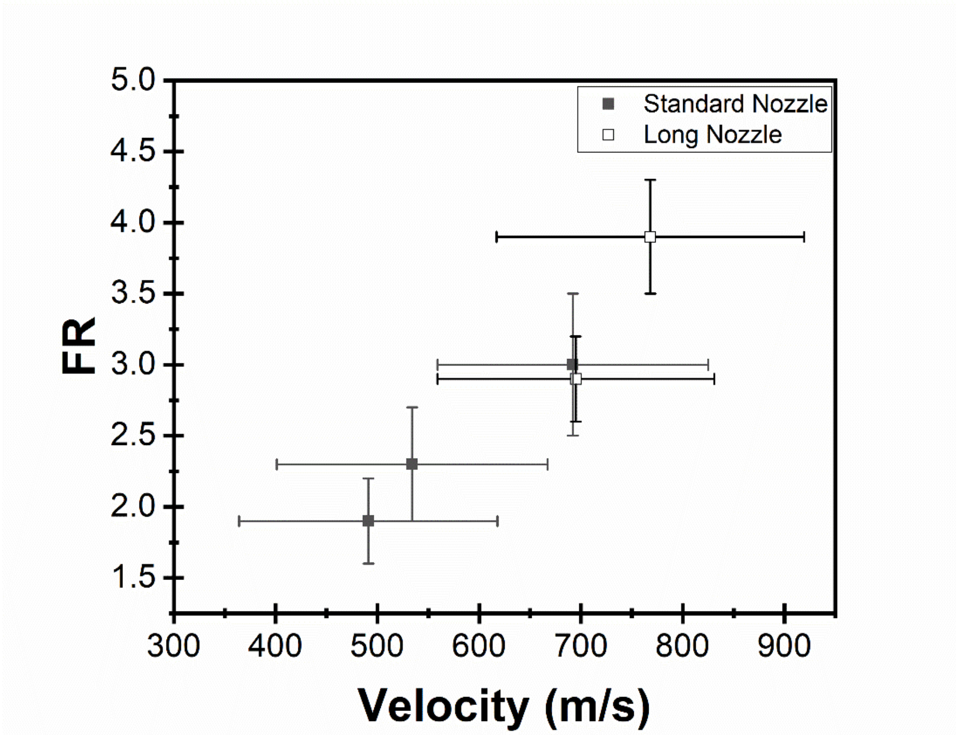

Standard Nozzle
Long Nozzle
FR
Velocity (m/s)
5.0
4.5
4.0
3.5
3.0
2.5
2.0
1.5
300
400
500
600
700
800
900


**Fig. 5.**

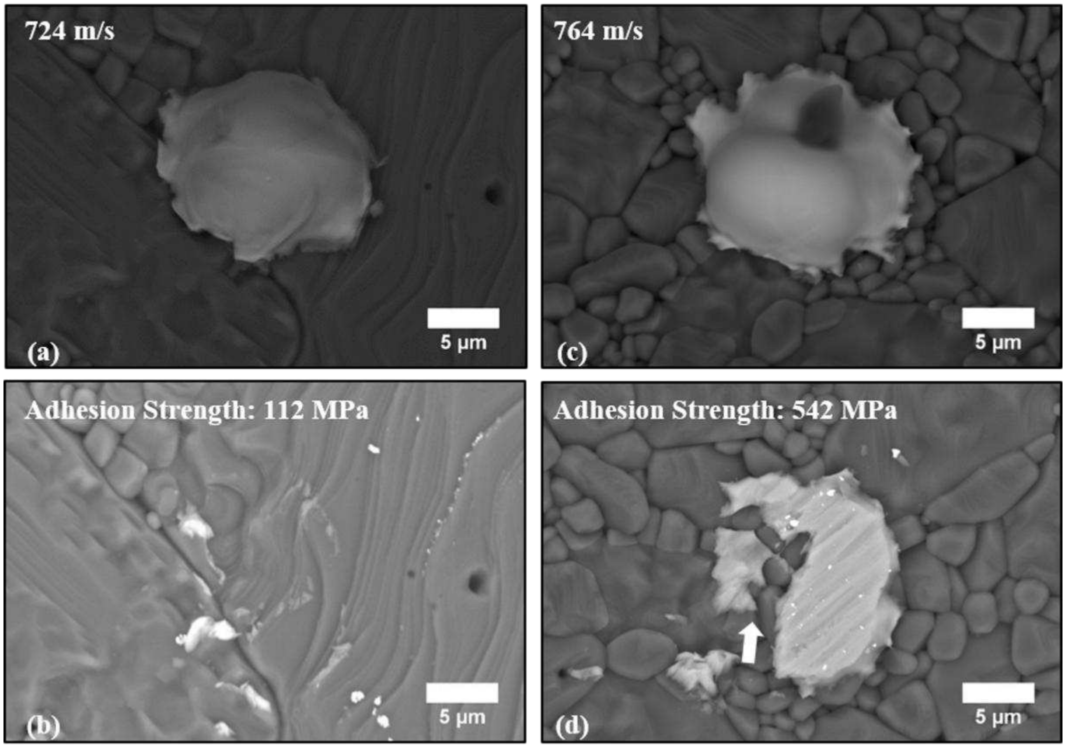
724 m/s
5 µm
(a)
764 m/s
5 µm
(c)
Adhesion Strength: 112 MPa
5 µm
(b)
Adhesion Strength: 542 MPa
5 µm
(d)

**Fig. 6.**

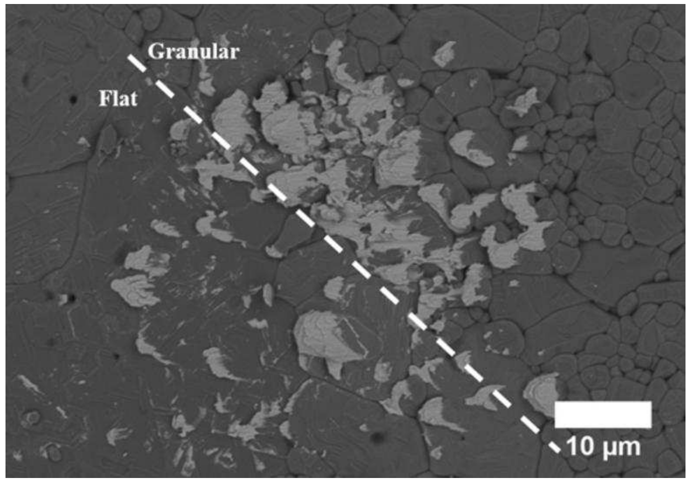


**Fig. 7.**

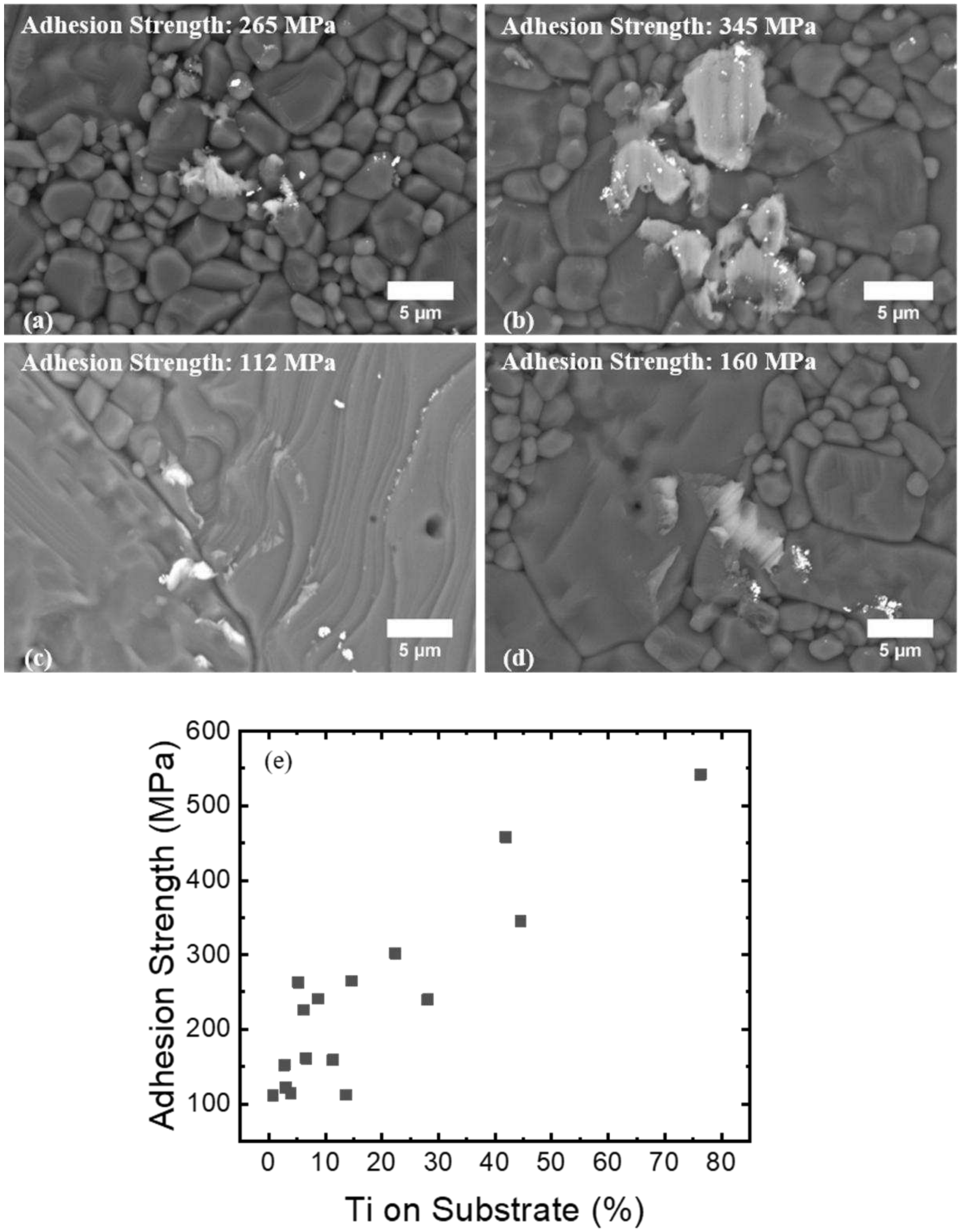
Adhesion Strength: 265 MPa
5 µm
(a)
Adhesion Strength: 345 MPa
5 µm
(b)
Adhesion Strength: 112 MPa
5 µm
(c)
Adhesion Strength: 160 MPa
5 µm
(d)
(e)
Adhesion Strength (MPa)
600
500
400
300
200
100
0
10
20
30
40
50
60
70
80
Ti on Substrate (%)

**Fig. 8.**

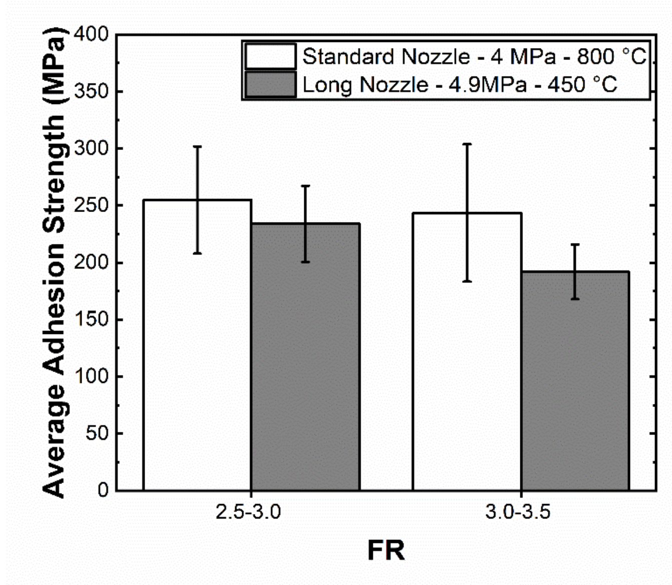
Standard Nozzle - 4 MPa - 800 °C
Long Nozzle - 4.9MPa - 450 °C
Average Adhesion Strength (MPa)
400
350
300
250
200
150
100
50
0
2.5-3.0
3.0-3.5
FR

**Fig. 9.**

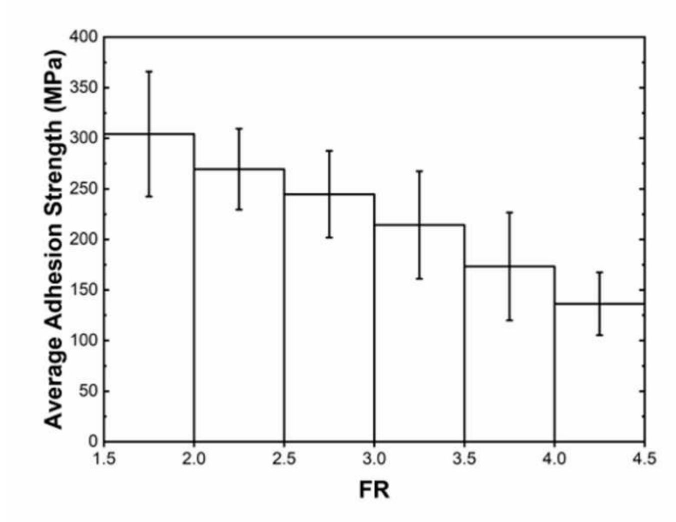
Average Adhesion Strength (MPa)
FR
0
50
100
150
200
250
300
350
400
1.5
2.0
2.5
3.0
3.5
4.0
4.5

**Fig. 10.**

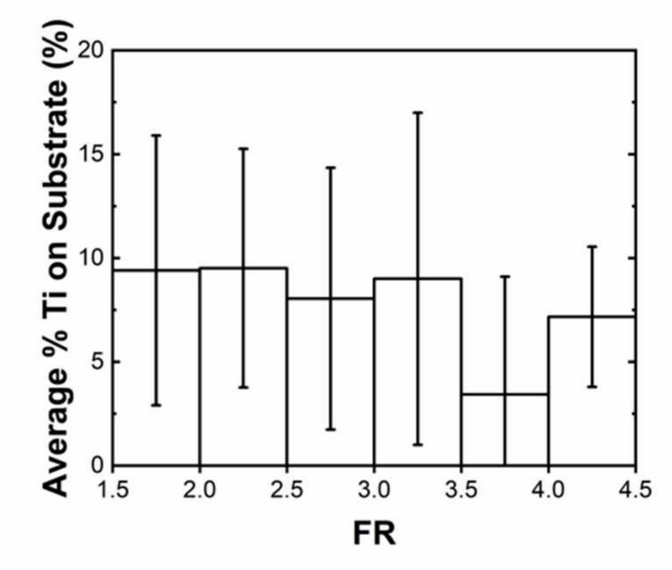


**Fig. 11.**

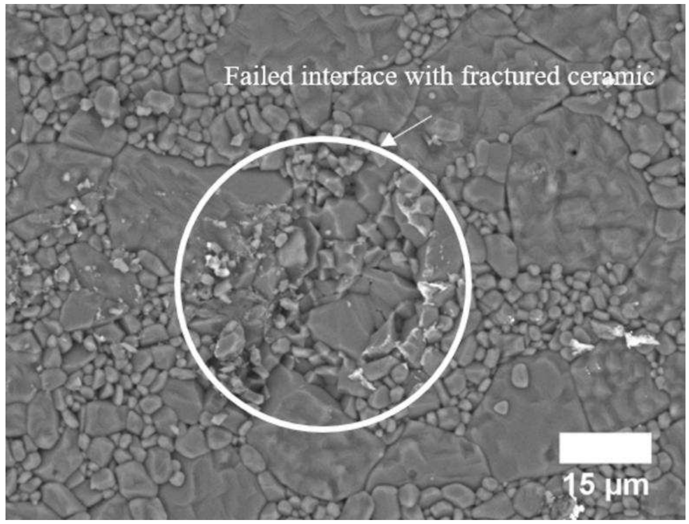


**Fig. 12.**

**Table**

**Table I**

Experimental average particle velocity and modeled particle temperature for powder particles deposited by cold spray under different spray conditions

| Nozzle Geometry | Spray Conditions | Experimental Average Particle Velocity (m/s) | Modeled Particle Temperature at Exit of Nozzle (℃) |
|---|---|---|---|
| Standard Nozzle | 4.0 MPa, 400°C | 491 ± 127 | 183 |
| Standard Nozzle | 4.0 MPa, 600°C | 543 ± 133 | 322 |
| Standard Nozzle | 4.0 MPa, 800°C | 692 ± 133 | 459 |
| Long Nozzle | 4.9 MPa, 450°C | 695 ± 136 | 166 |
| Long Nozzle | 4.9 MPa, 800°C | 768 ± 151 | 343 |

Figure
Click here to download high resolution image

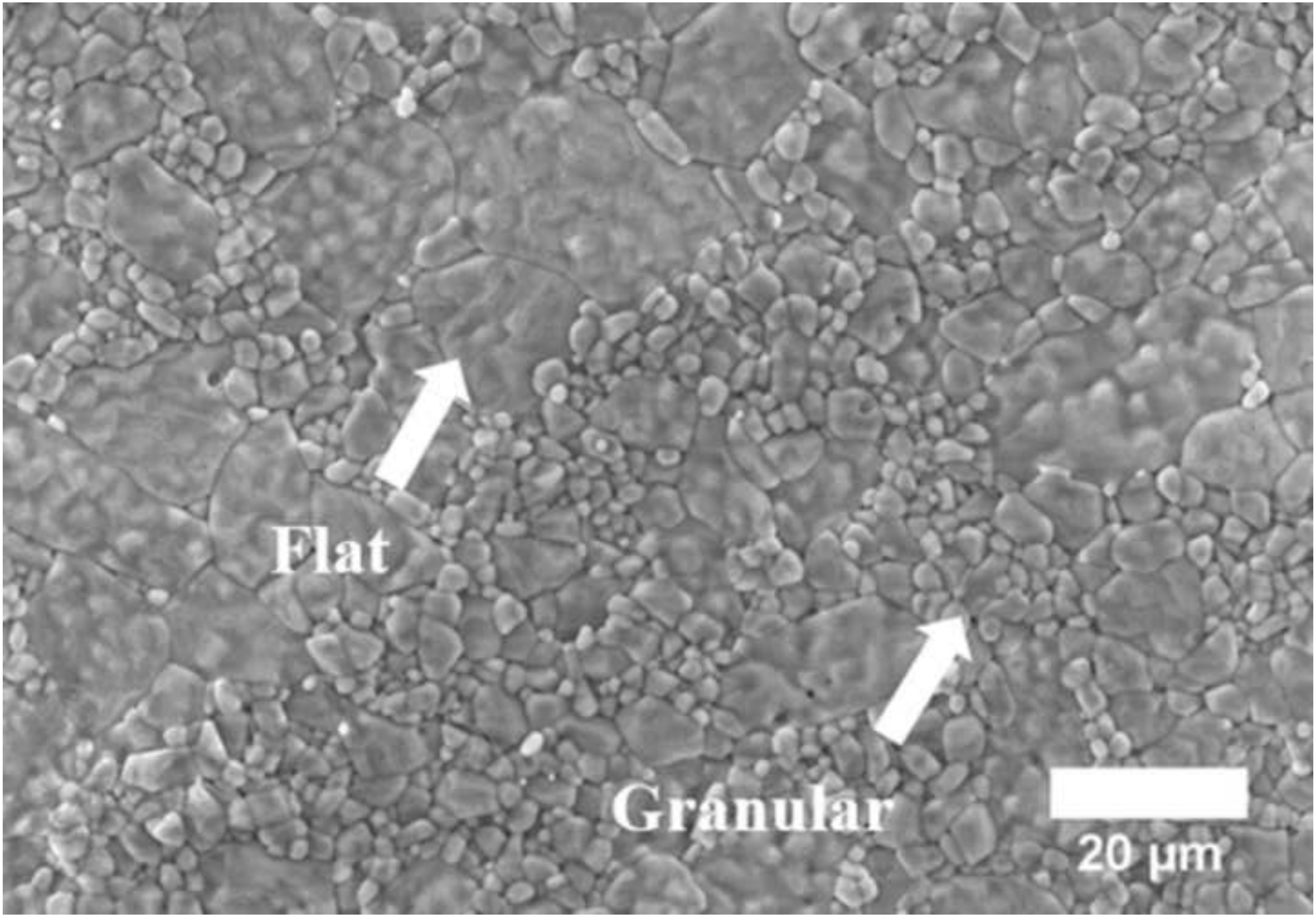

Figure

Click here to download high resolution image

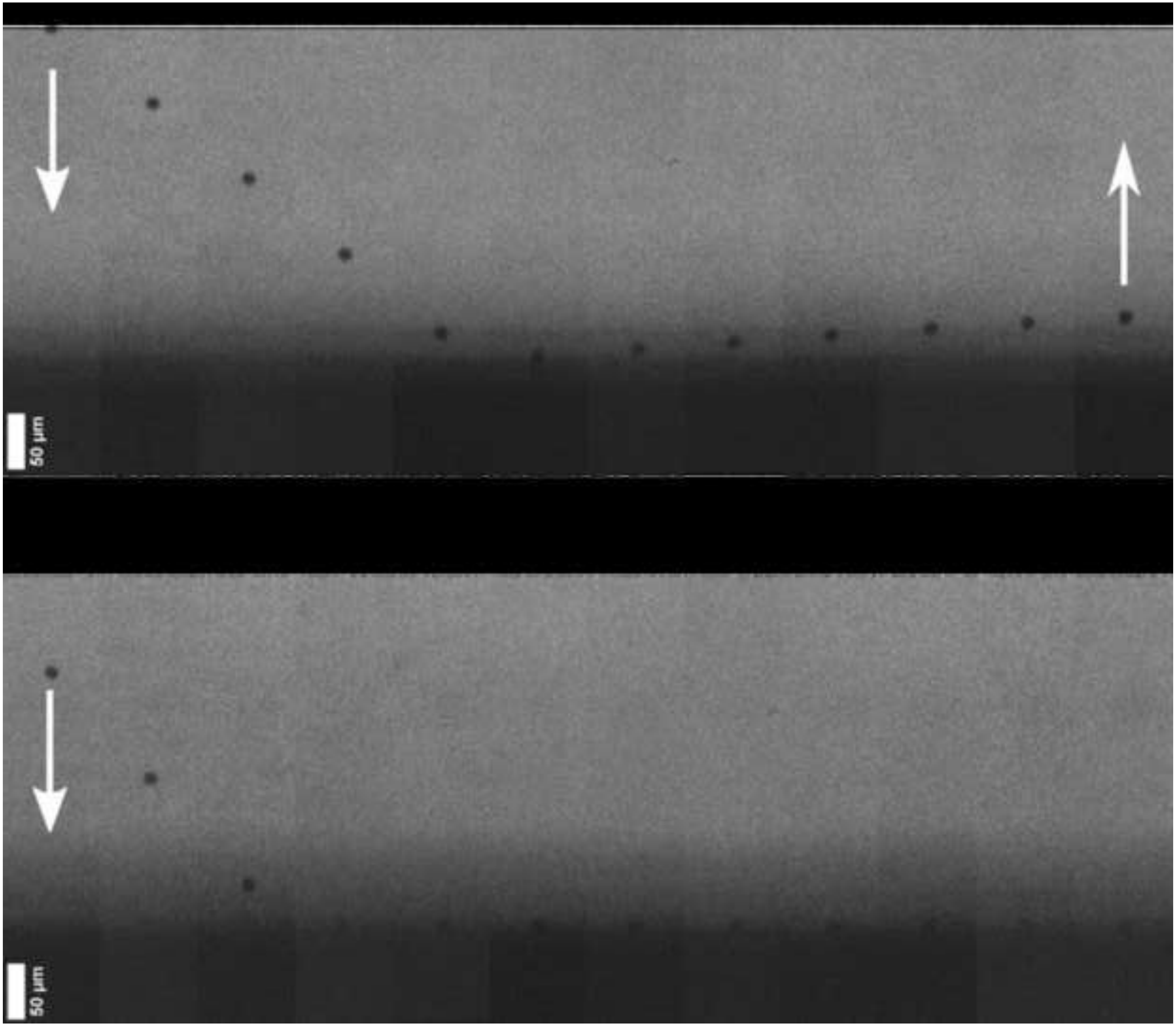

Figure


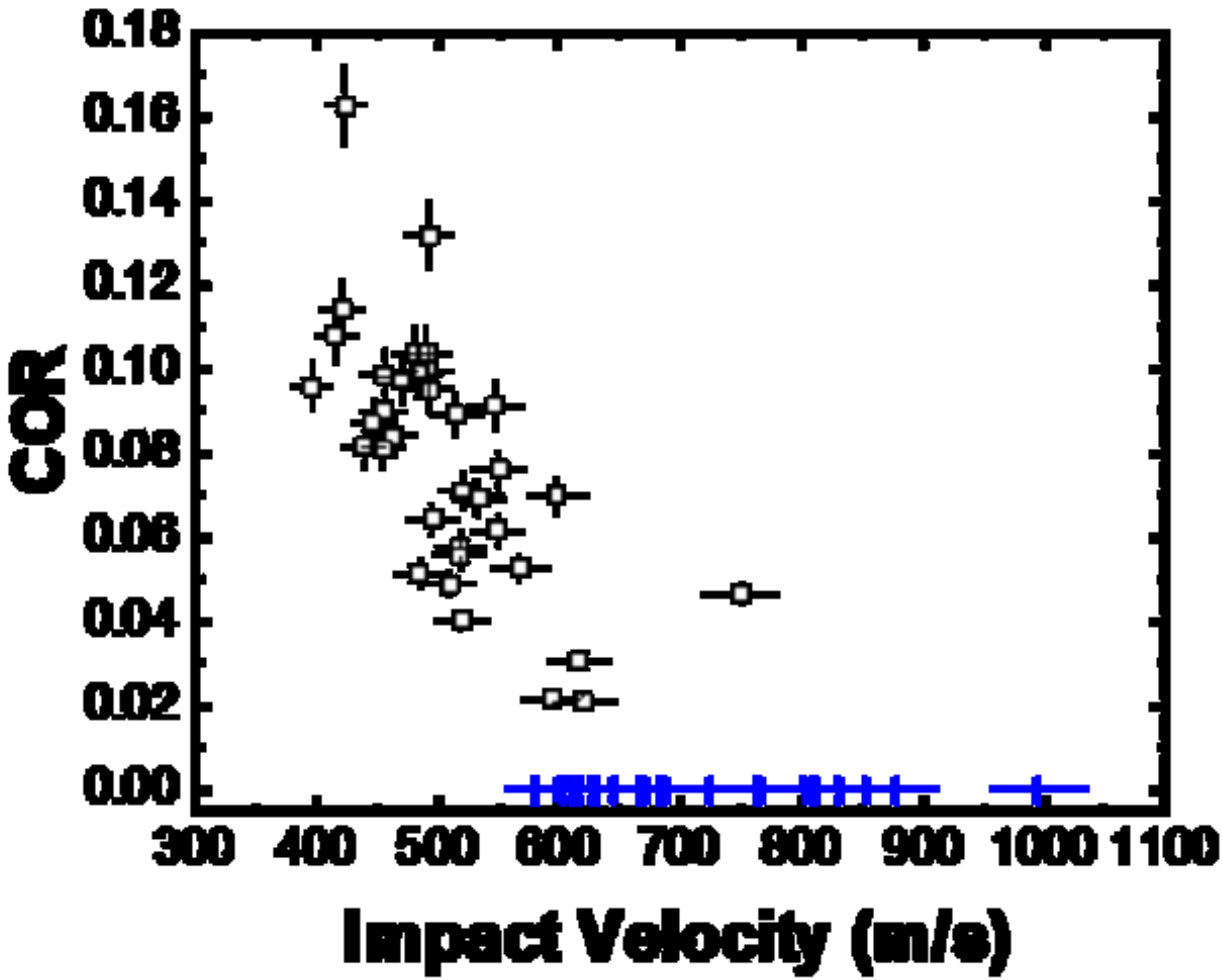
0.18
0.16
0.14
0.12
0.10
0.08
0.06
0.04
0.02
0.00
COR
300
400
500
600
700
800
900
1000
1100
Impact Velocity (m/s)

Figure
Click here to download high resolution image

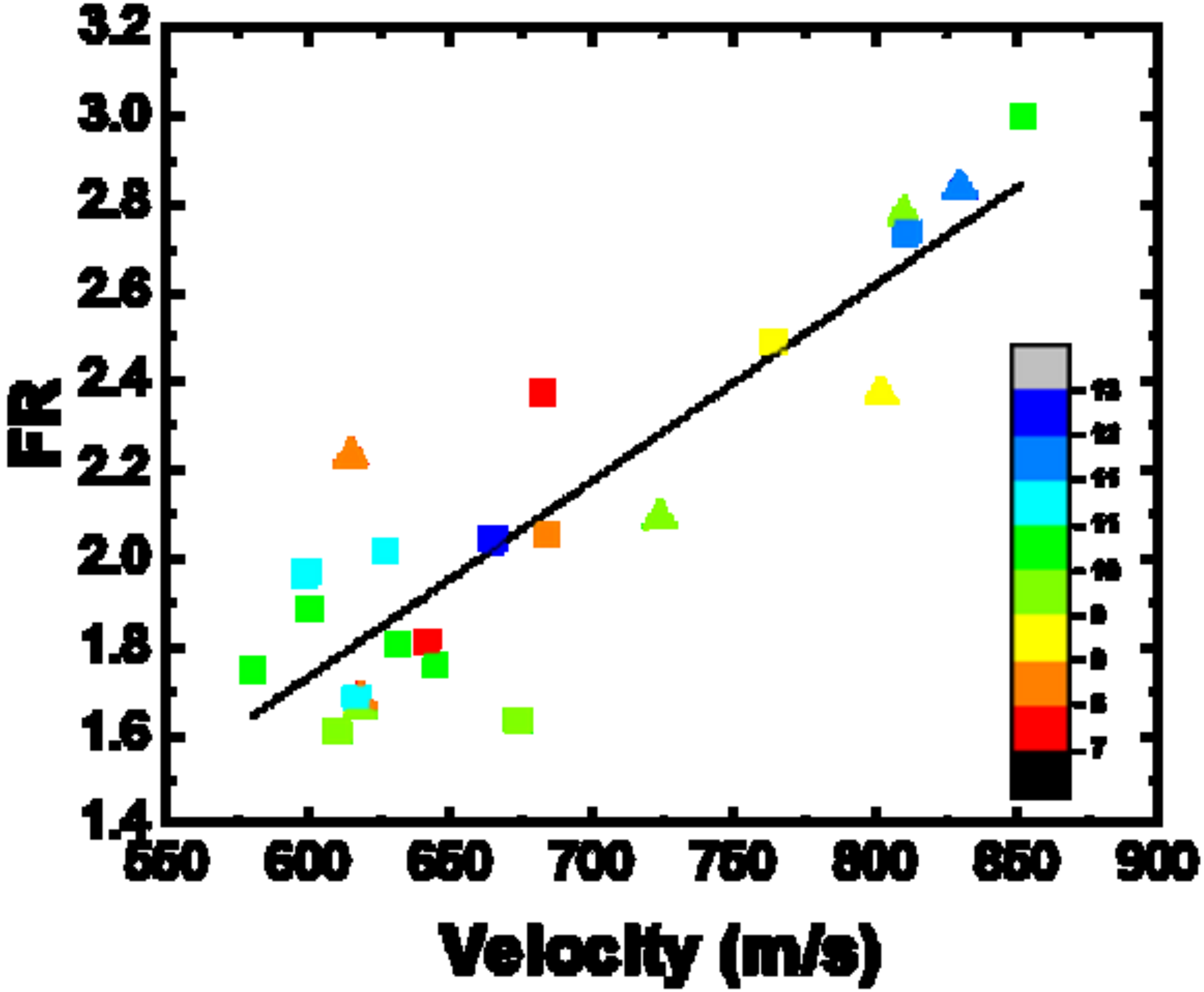

Figure
Click here to download high resolution image

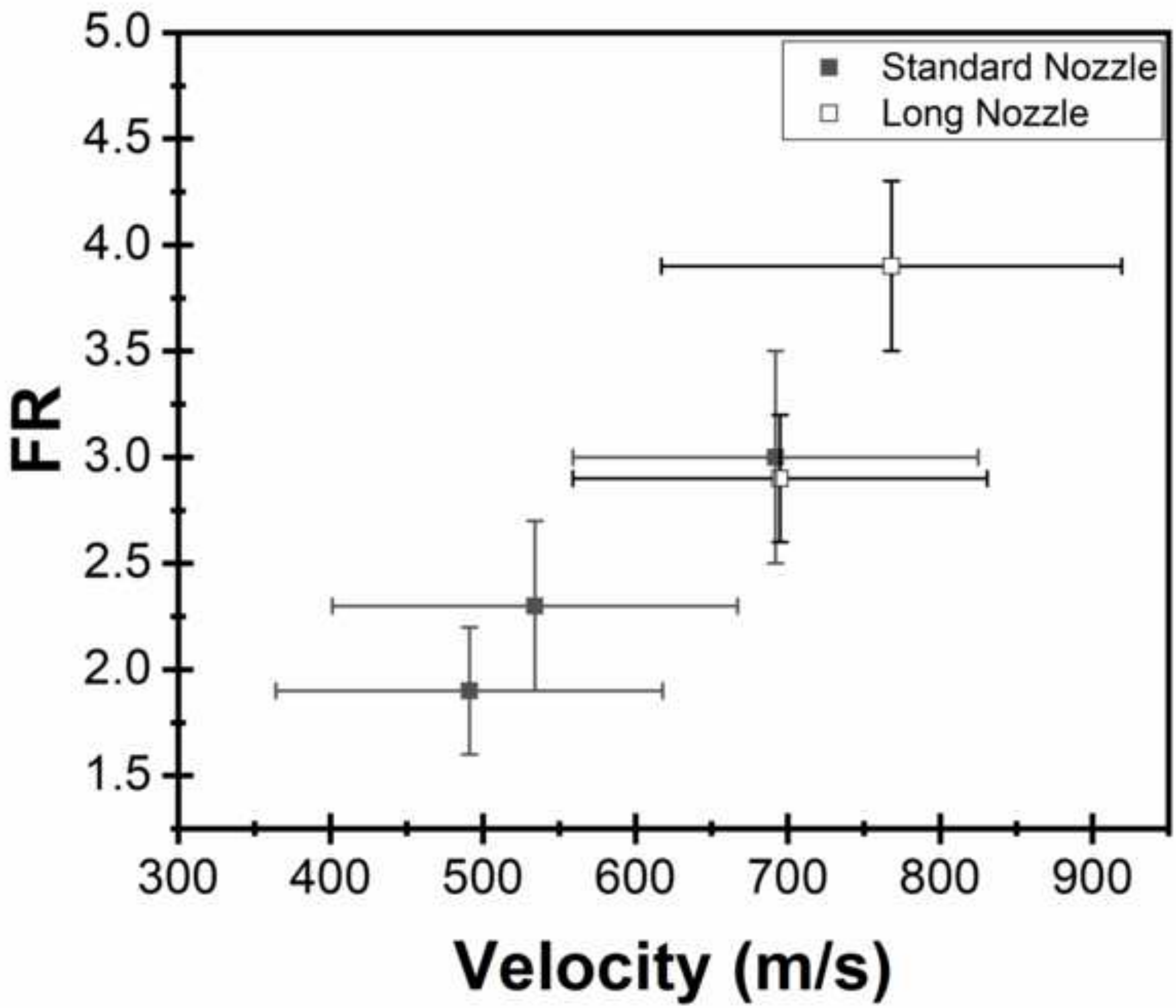

Figure
Click here to download high resolution image

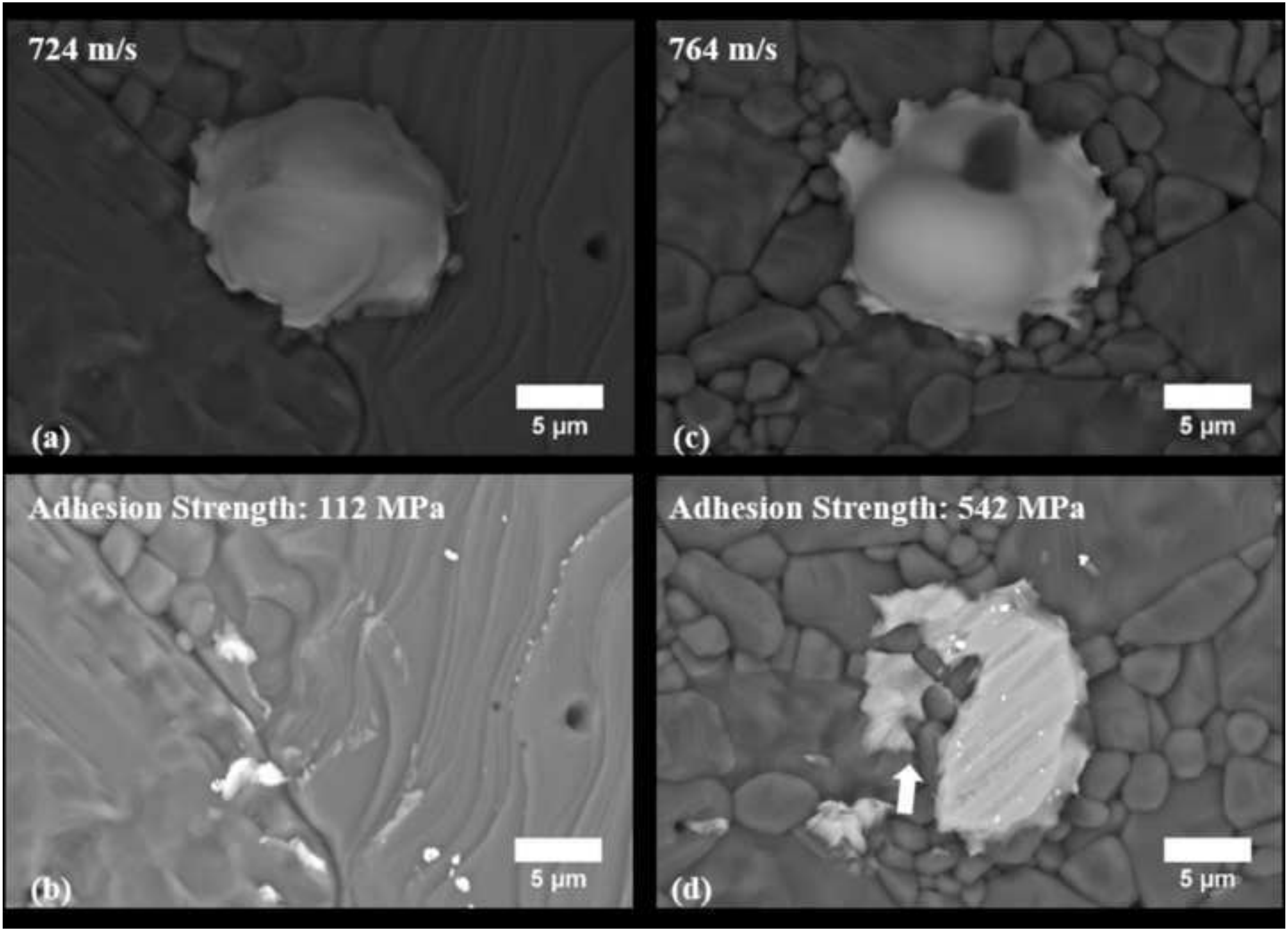

Figure
Click here to download high resolution image

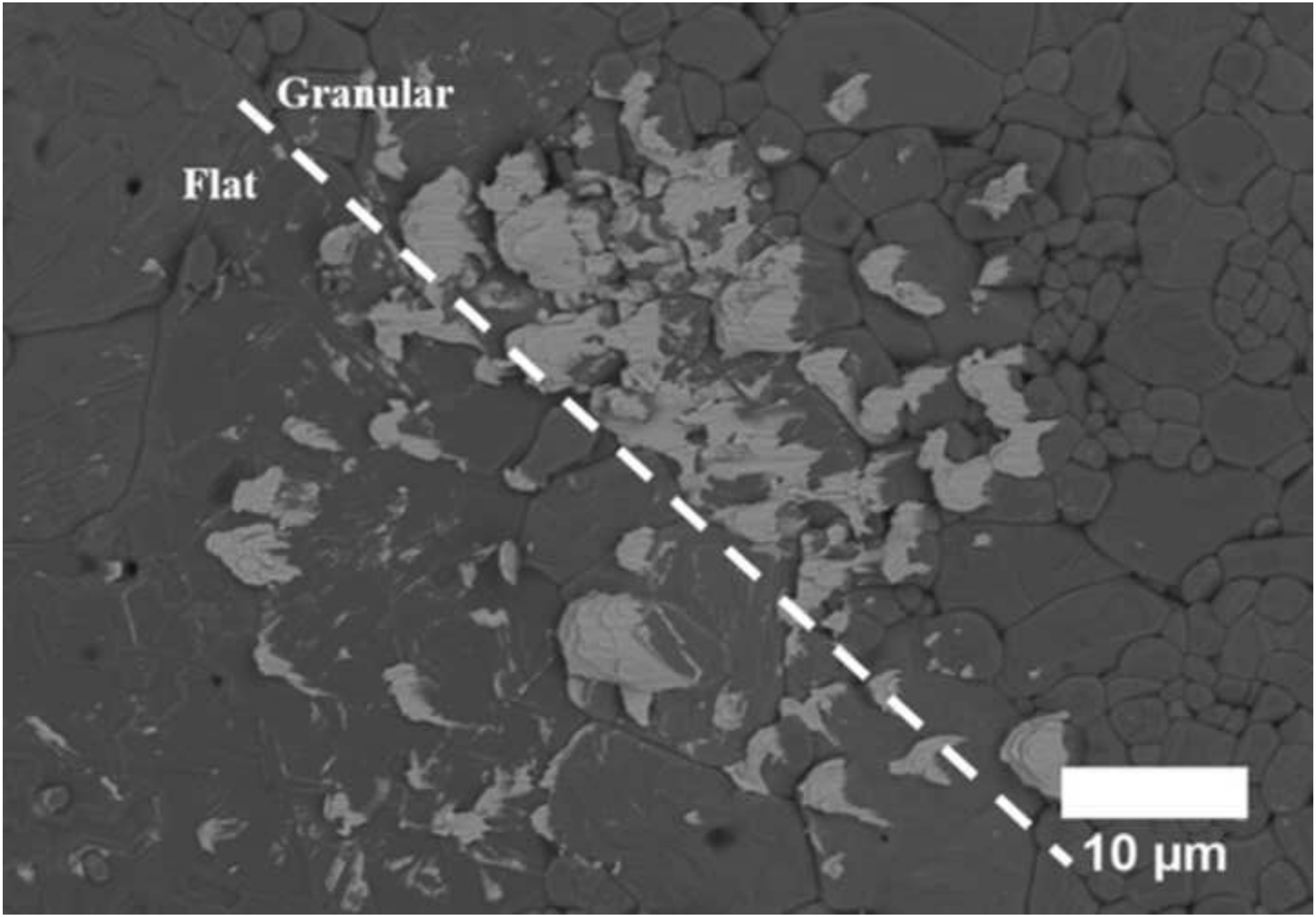

Figure
Click here to download high resolution image

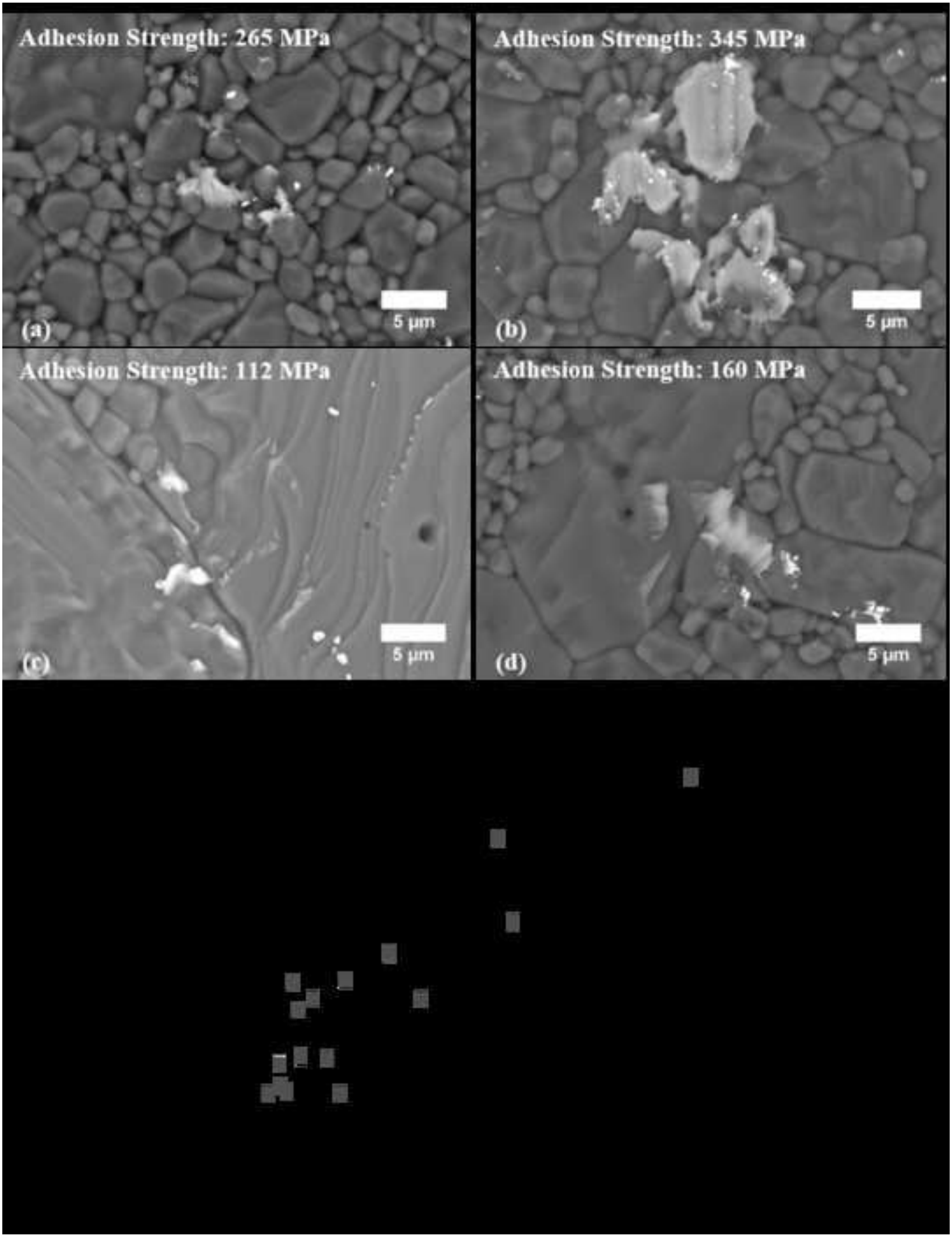

Figure
Click here to download high resolution image

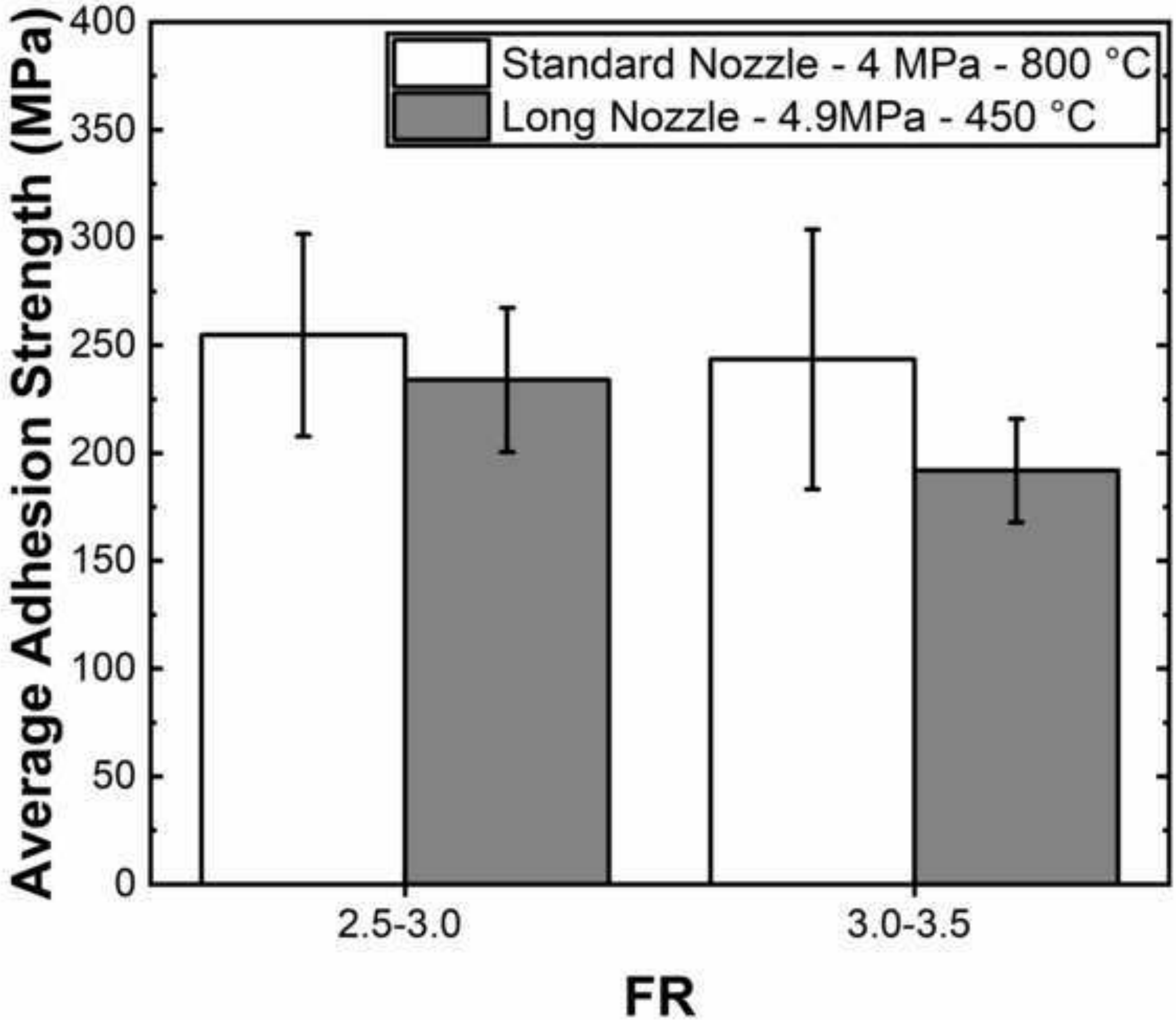

Figure
Click here to download high resolution image

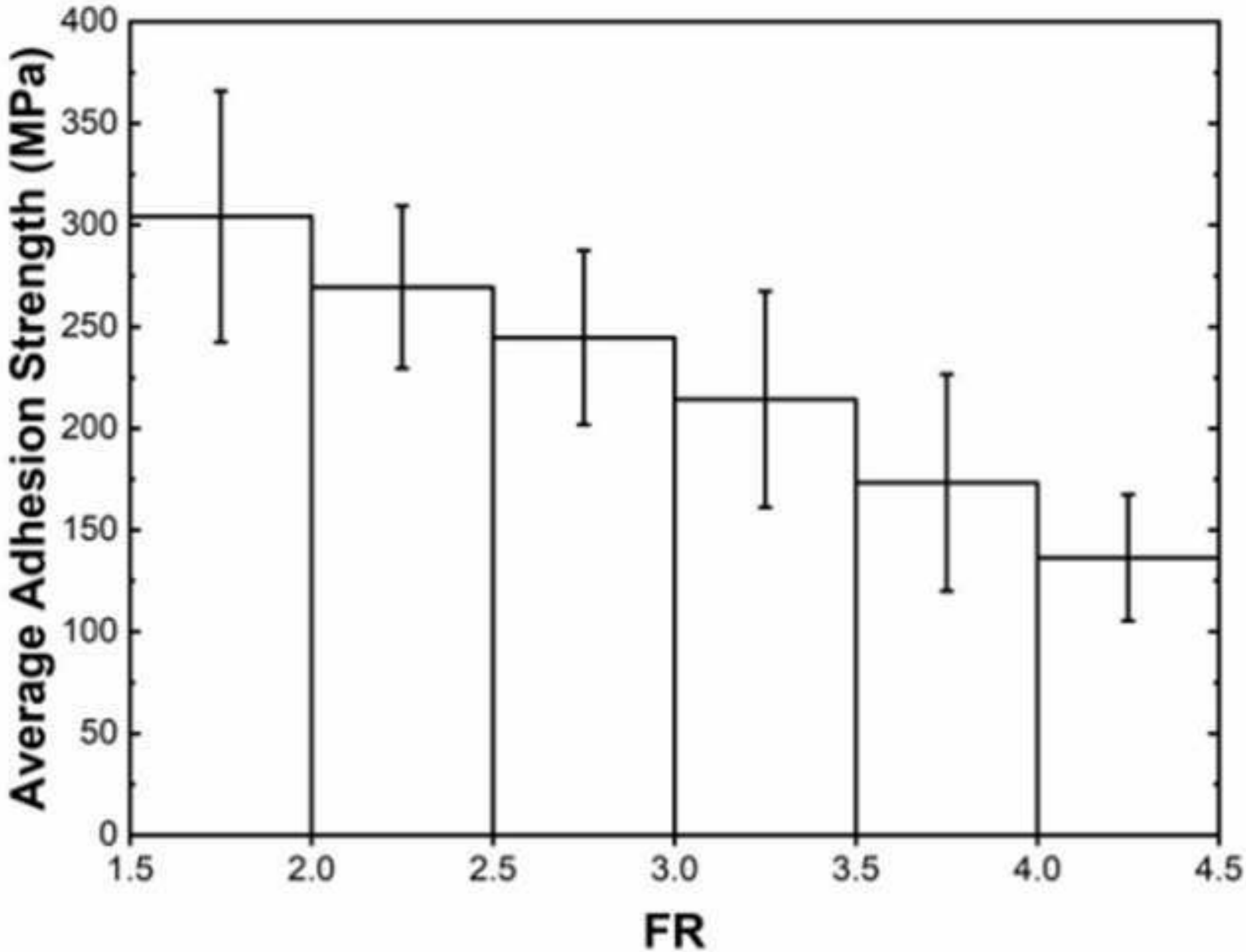

Figure
Click here to download high resolution image

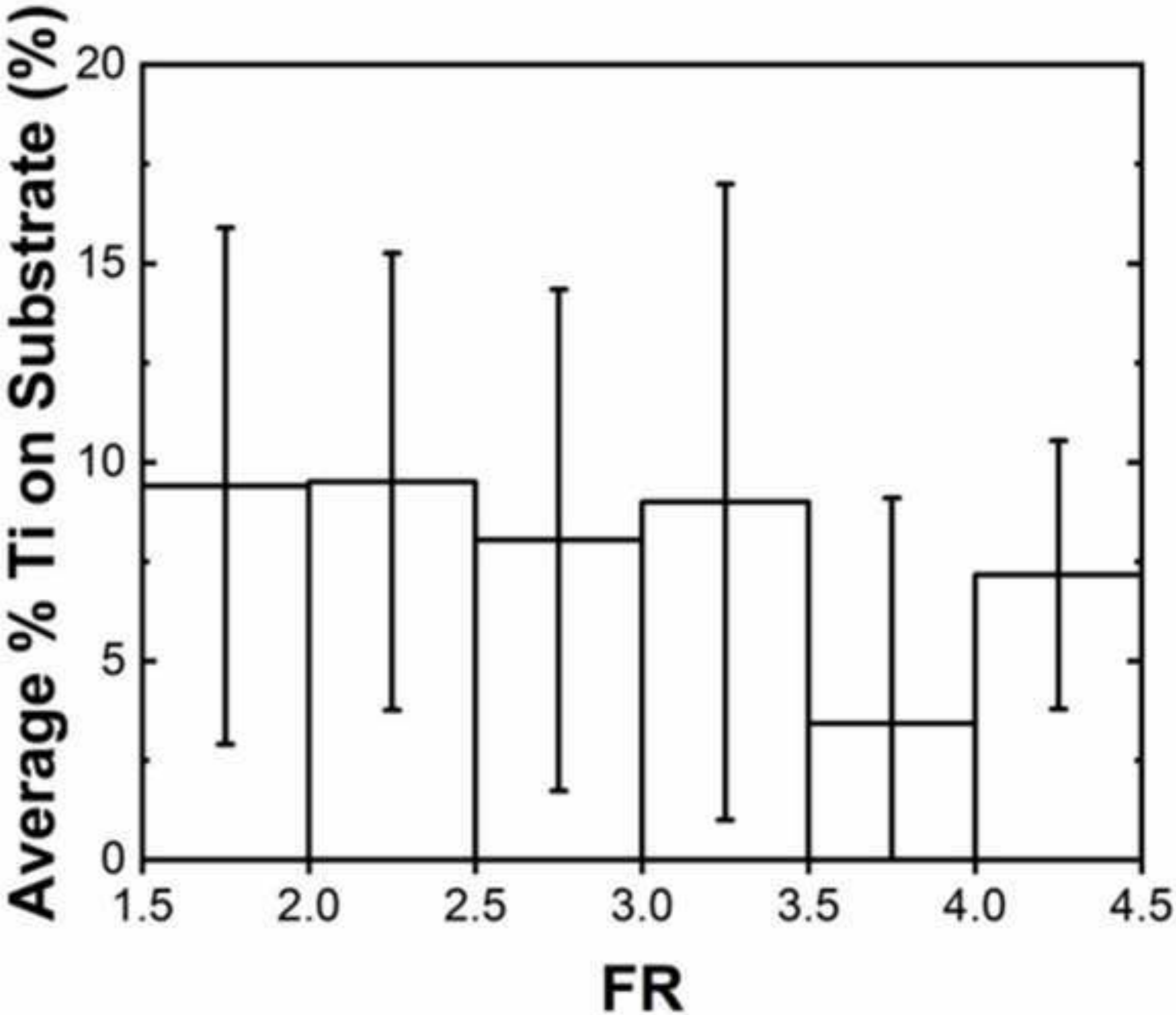

Figure
Click here to download high resolution image